4. CdTe/CdS RESEARCH

4.1 SUMMARY

4.1.1 CdTe/CdS Device Performance

In this reporting period vapor phase $CdCl_2$ treatments were developed, permitting the effects of reaction temperature and chloride concentration on materials and devices to be investigated. Vapor $CdCl_2$ treatment at 420˚C was found to result in uniform modification of the film properties. Combined with the contacting process developed in the previous reporting period, the uniform and reproducible treatments have translated into greater consistency in device performance at an efficiency level of 12% [401] The J-V curve of such a cell is shown in Figure 4-1. The V_{OC} is approaching state-of-the-art values, but J_{sc} and FF are low. The resistance at V_{OC} in these devices is in the range of 6 to 10 Ω-cm^2. Reducing this to 1–2 Ω-cm^2 by optimizing the CdTe doping and contact are expected to increase FF to >72% and should enhance the V_{OC}. Control over S interdiffusion with vapor treatment and use of alloyed films is described in the sections below and offers several avenues for improving J_{SC}: 1) use thick CdS (~250 nm) and high S diffusion process to thin down the CdS, boosting J_{SC} contributions from 300–550 nm and 750–900 nm; 2) use ultrathin CdS (<50 nm) and low S diffusion process to minimize loss of CdS film; and 3) deposit $CdTe_{1-x}S_x$ films with x near the solubility limit on ultrathin CdS to minimize driving force for interdiffusion.

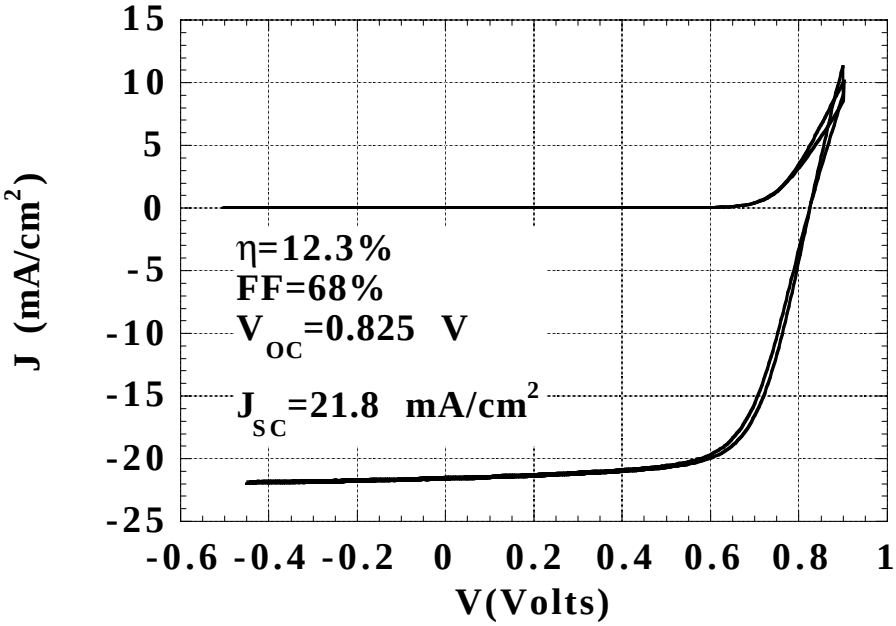

Figure 4-1. J-V curve of PVD CdTe/CdS device 40926.11-3 processed with $CdCl_2$ vapor (using a coated plate as the vapor source).

4.1.2 $CdCl_2$ Treatment

All-vapor post deposition processing holds many advantages the over conventional coat-and-rinse techniques that are employed for CdTe cells [402, 403]. For example, the thermal separation of CdTe/CdS films from the chloride source allows independent control of both the reaction temperature and species concentration. This facilitates temperature-time configurations that: can reduce the CdS loss via interdiffusion; increase the V_{OC}; reduce the treatment time; and produce a residue-free CdTe surface. Figure 4-2 shows the CdTe (511) XRD peak profile in 2.5 µm CdTe/0.2 µm CdS structures after $CdCl_2$ vapor treatment. The bimodal profile obtained for the sample in which the $CdCl_2$ and CdTe/CdS structure were heated together indicates extensive CdTe-CdS mixing and corresponds to an equivalent CdS thickness of approximately 65 nm. Delaying the delivery of $CdCl_2$ vapor by two minutes after reaching reaction temperature results in a diffusion tail that corresponds to an equivalent CdS thickness of less than 20 nm.

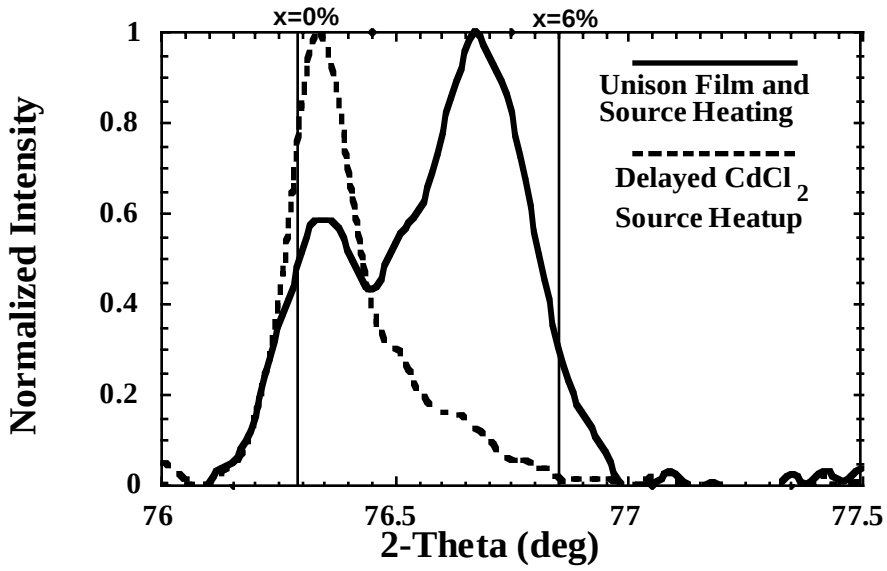

Figure 4-2 $CdTe_{1-x}S_x$ (511) XRD profile for CdTe/CdS structures heated in unison with (solid) and prior to (dotted) the $CdCl_2$ source.

The vapor chloride processing yields a spatially uniform grain size and a clean CdTe surface free of residual chlorides, oxides, and chlorates. This eliminates the necessity for rinsing or handling of rinsates prior to contact formation. From a device perspective, these benefits translate into spatially uniform properties and performance. Table 4-1 shows the current-voltage parameters for four 0.2 cm^2 area cells fabricated on a 1” x 1” sample processed with $CdCl_2$ vapor treatment.

Table 4-1. Current-voltage parameters for CdTe/CdS cells demonstrating spatial uniformity of device performance with vapor chloride processing.

Cell	V_{OC} (mV)	J_{SC} (mA/cm^2)	FF (%)	Eff (%)
1	786	21.4	67	11.2
2	795	21.8	64	11.1
3	779	21.0	66	10.8
4	790	21.5	66	11.2

The role of $CdCl_2$ in promoting recrystallization, grain growth and interdiffusion between CdS and CdTe layers in physical vapor deposited CdS/CdTe thin film solar cells is has been examined[404]. CdTe/CdS thin film samples prepared with different CdTe film thicknesses and treated in air at 415˚C for different times with and without a surface coating of $CdCl_2$. The samples were characterized by scanning electron microscopy, transmission electron microscopy, energy dispersive x-ray spectroscopy, x-ray diffractometry, and optical absorption. The results show that $CdCl_2$ treatment enhances the recrystallization and diffusion processes, leading to a compositional variation within the CdTe layer due to diffusion of S from the CdS. The highest S concentrations observed, after 30 minute treatments with $CdCl_2$ at 415˚C, are near the solubility limit for S in CdTe. The compositional distributions indicated by x-ray diffraction measurements of samples with different CdTe thickness show that the S-rich $CdTe_{1-x}S_x$ region lies near the CdTe-CdS interface. A multiple step mixing process must be inferred to account for the diffraction profiles obtained.

4.1.3 CdTe-CdS Alloys and Devices

The CdTe-CdS alloy system has been characterized at typical solar cell processing temperatures in order to elucidate the role of interdiffusion in CdTe/CdS-based solar cells [405, 406]. Predominately single phase $CdTe_{1-x}S_x$ thin films with x∫[S]/([S]+[Te]) ranging from 0 to 0.45, were grown by vacuum co-evaporation of CdS and CdTe. Phase segregation was promoted by heat treatment of the films at 415°C in the presence of $CdCl_2$. The solubility limits of S in CdTe and Te in CdS at 415°C were derived by measuring the compositions of the two phases in the films after the $CdCl_2$ treatment. The solubility limit of S in CdTe was determined to be 5.8%. Solar cells were fabricated with compositionally uniform absorber layers of $CdTe_{1-x}S_x$ with x near the solubility limit before heat treatment. An efficiency of 10.8% was achieved by a $CdTe_{1-x}S_x$/CdS device. The V_{OC}, J_{SC}, FF and spectral response of this device were all very similar to vacuum evaporated conventional CdTe/CdS cells where the alloy is formed by diffusion of S during cell processing.

4.1.4 HCl Vapor Treatment

Data on the structural and optical properties and cell performance of thermally evaporated CdTe/CdS films were determined as functions of the HCl concentration and temperature of a post-deposition heat treatment [407]. The degree of preferred (111) orientation decreased while the grain size of the CdTe films increased with increasing HCl concentration and temperature. The sulfur content of a $CdTe_{1-x}S_x$ layer also increased with HCl concentration and temperature to a maximum value of ~2%. Cell performance improved over as-deposited values to ~8% efficiency.

4.1.5 Stress Testing of CdTe/CdS Devices

CdTe/CdS solar cells have been known to exhibit various combinations of reversible and irreversible degradation of conversion efficiency after being subjected to temperature, voltage and illumination at levels which equal or surpass those expected in field conditions[408]. This paper describes a series of measurements designed to quantify these phenomena. The QE and light and dark J-V characteristics of a set of CdTe devices were measured, then devices were subjected to various combinations of stresses within the parameter space of 0-70 mW/ cm^2 illumination, -0.5 V to +5 mA/ cm^2 electrical bias, and temperatures from 72˚ to 112˚C. The device characteristics were measured and changes are interpreted in the context of an equivalent circuit which includes the effects of both the main junction diode, series resistor and a rectifying back contact.

4.2 $CdCl_2$ TREATMENT

4.2.1 Vapor $CdCl_2$ Treatment

4.2.1.1 Introduction

Several approaches to fabricate high efficiency CdTe/CdS thin film solar cells rely on post deposition heat treatment of the CdTe/CdS structure by $CdCl_2$ in air to enhance the device performance [409-412]. The treatment usually consists of coating the CdTe surface with a saturated solution of $CdCl_2$ in methanol, drying, heat treating the $CdCl_2$/CdTe/CdS structure in air at ~400˚C for 10 to 30 minutes, and rinsing or etching the structure prior to the contacting process. This approach is susceptible to spatial variability and irreproducibility depending on the uniformity of the $CdCl_2$ layer produced by the wet application technique [413](pp. 69-74). Module fabrication processes would have to contend with the application, recovery and recycling of the $CdCl_2$ containing solutions. Further, analytically quantifying the action of the $CdCl_2$ on the CdTe/CdS structure is limited by the coupling of the $CdCl_2$ concentration and the reaction temperature.

Previously, we have demonstrated that physical vapor deposited CdTe films could be recrystallized by $CdCl_2$ vapor at 25 torr with a CdTe and $CdCl_2$ separation of several centimeters [414] (pp. 42-46). The reaction uniformly recrystallized the CdTe films and produced devices having 9-10% efficiency. The experimental configuration, however, did not allow determination of the $CdCl_2$ vapor phase concentration at the CdTe surface. Zhou, et. al. [415] demonstrated >10% efficient devices using a vapor treatment with either $CdCl_2$ or HCl on CdTe/CdS deposited by a high temperature process. More recently we demonstrated that >10% efficient devices could be achieved by treatment at atmospheric pressure by placing the $CdCl_2$ in close proximity to the CdTe surface [416]. This configuration does not permit the variation of the parameters over a wide range because the $CdCl_2$ vapor phase concentration is fixed by the CdTe temperature. In the present work a new approach is described which overcomes these limitations and which allows the critical treatment parameters to be studied in detail.

4.2.1.2 Experimental

Thin films of CdTe and CdS were grown on In_2O_3:Sn (ITO) coated 7059 glass by thermal evaporation from CdTe source powder. Prior to CdTe deposition the 0.2 µm thick CdS films were heat treated with $CdCl_2$ vapor to reduce optical absorption and to minimize diffusion of Te into CdS during subsequent processing [417].

The treatments were performed by exposure of the CdTe/CdS films to vapor generated from a powder $CdCl_2$ source in a quartz reactor fitted with temperature controlled graphite susceptors

heated externally by FCM lamps in linear housings. The $CdCl_2$ source powder was evenly distributed in a graphite susceptor supported on a quartz frame with a milled central cavity. A mica mask was used as both a separator and radiative/thermal insulator between the source susceptor and the thin film sample. A second graphite susceptor rested on top of the thin film sample to provide independent heating control. Using a CdTe/CdS/ITO/glass sample with an embedded microthermocouple, the time needed to heat the sample to 400˚C was measured to be 40 seconds. The time to heat the $CdCl_2$ susceptor to 400˚C was measured to be 20 seconds. Thus, the heatup rate of the susceptors, not the characteristic diffusion times (~2 sec), controls the time to reach equilbrium conditions in the reaction zone.

Evaluation of the effects of $CdCl_2$ vapor phase concentration and reaction temperature was made by independently controlling the temperatures of the thin film (T_f) and the $CdCl_2$ source (T_S): 1) $T_f > T_S$; 2) $T_f = T_S$; 3) $T_f < T_S$ (CSVT mode). Two types of heating profiles were employed: delayed heating to allow the CdTe/CdS sample to reach thermal equilibrium before the $CdCl_2$ and unison heating to simulate the conditions of $CdCl_2$-coated samples. To prevent $CdCl_2$ condensation on the CdTe/CdS in cases 1 and 2 due to mismatched heating rates, the CdTe/CdS was heated prior to and cooled after the $CdCl_2$. Atmospheric pressure treatments were conducted under flowing gas at a total flow rate of 0.94 l/m at one atmosphere total pressure. The system was pumped to < 50 mTorr prior to backfilling, which, for vacuum and argon treatments established a maximum oxygen partial pressure of <10 mTorr.

Film surface morphology and average grain size (AGS) were assessed by scanning electron microscopy (SEM). Energy dispersive spectroscopy (EDS) was used to examine the chemical composition of the CdTe surface after treatments. Optical transmission and reflection were measured in the wavelength region near the CdTe bandedge for evidence of S diffusion into CdTe. Scanning x-ray diffraction (XRD) patterns of the films were taken with Cu ka radiation using Bragg-Bretano focusing geometry to determine the normalized (111) orientation parameter, p(111) [418] and the precision lattice parameter [419]. High resolution x-ray diffraction scans of high order (hkl) reflections were made to assess alloying between CdTe and CdS. To maximize detection sensitivity of the thin layers at the CdS-CdTe interface, the absorptive loss of signal in the overlying CdTe was overcome by using films thinner than the penetration depth for that x-ray energy and Bragg angle. Either ~2.5μm thick CdTe films were employed, or thicker films (4-5 μm) were thinned after processing by a polishing etch with a buffered solution of $K_2Cr_2O_7$:H_2SO_4, such as Dichrol. Devices were completed by use of the diffused copper contacting process described elsewhere [420]. Light and dark current-voltage (J-V) traces and quantum efficiency measurements were used to determine conversion efficiency and spectral response changes within the devices.

4.2.1.3 Estimation of $CdCl_2$ Vapor Concentration

To understand the behavior of the gases in the reaction zone, the mass and thermal diffusion characteristics were determined for the reactor geometry in all thermal modes of operation. The results of this modelling show that the characteristic times to reach thermal equilibrium in air at 1 atm and mass transfer equilibrium are less than 2 seconds for isothermal reactions with a 2 mm separation between sample and $CdCl_2$ surface at 400˚C, assuming no mass transport out of the reaction zone. Table 4-2 lists the $CdCl_2$ equilibrium vapor phase concentration, number of collisons with CdTe surface per unit area per second, and the saturation pressure [421] for the temperatures listed in the reaction zone.

Thermometric and gravimetric measurements of the source and substrates in isothermal mode verify the assumptions of the model. In CSVT mode at T_S=420˚C and T_f=320˚C the $CdCl_2$ deposition rate on glass agreed with the model prediction, providing a check on the assumption that

the $CdCl_2$ powder reaches the susceptor set point temperature.

Table 4-2 $CdCl_2$ vapor phase heat treatment reactor equilibrium conditions for isothermal reactions.

T $CdCl_2$ (˚C)	[$CdCl_2$] at CdTe x10^{-10} (mol/cm^3)	Surface Collisions x10^{17} (#/cm^2/s)	P_{sat} (mTorr)
380	0.325	1.35	1.3
410	1.33	5.62	5.7
420	2.06	8.79	9.0
430	3.16	1.36	14.0
450	7.15	31.1	32.7

4.2.1.4 Material Results

4.2.1.4.1 Thermal Effects

Table 4-3 presents the materials data for treatments conducted in bottled air under isothermal, $T_f = T_S$, and other thermal conditions. Isothermal treatments with delayed heating at 380˚C, 410˚C, 420˚C and 430˚C show increasing grain size with temperature as has been observed for the $CdCl_2$:methanol method [421]. The grain structure and morphology obtained after vapor treatment at 410˚C and 430˚C for 20 minutes are shown in Figure 4-3. EDS of the surfaces showed no evidence of residual Cl. The extent of S diffusion, even at 430˚C, is substantially less than that obtained by the $CdCl_2$:methanol method at 410-420˚C.

Fixing the $CdCl_2$ concentration at 1 mTorr and increasing the reaction temperature from 380˚C to 450˚C resulted in progressive grain growth at 380˚C-420˚C but produced a two layer structure with underlying grains that are of comparable dimension to those found with the isothermal case at 420˚C. Fixing the reaction temperature at 420˚C but increasing the $CdCl_2$ concentration produced similar grain size to that obtained under isothermal conditions at 420˚C but, as expected, the surface was coated with dendritic clusters of $CdCl_2$ which rinsed away in methanol.

Table 4-3. Treatment conditions and materials results for 4.5 μm CdTe/0.2μm CdS films before and after processing by $CdCl_2$ vapor treatment. All samples were processed with delayed heating except the last.

T_f (˚C)	T_S (˚C)	t (m)	P_S (m Torr)	AGS (μm)	a_0 (Å) ±0.001	[S]/ [Te]+[S] (%)(±0.2)	p(111)
as dep	-	-	-	0.6	6.485	0	3.4
380	380	45	1.3	0.9	6.480	0.1	1.2
410	410	20	5.7	1.5	6.479	0.3	0.6
420	420	20	9.0	2.1	6.477	0.6	1.0
420	420	20	9.0	1.7	6.477	0.6	0.8
430	430	20	14.0	2.3	6.477	0.6	1.2
380	380	45	1.3	0.9	6.480	0.1	1.2
420	380	20	1.3	1.2	6.477	0.6	1.1
420	380	45	1.3	1.2	6.477	0.6	1.1
450	380	20	1.3	2.0	6.478	0.5	0.9
420	**380**	20	1.3	1.2	6.477	0.6	1.1
420	**420**	20	9.0	2.1	6.477	0.6	1.0
420	**450**	20	32.7	1.7	6.476	0.8	2.6
420	420	20	9.0	1.1	6.481	0.0	2.9
420	420	20	9.0	2.0	6.446	5.3	2.9

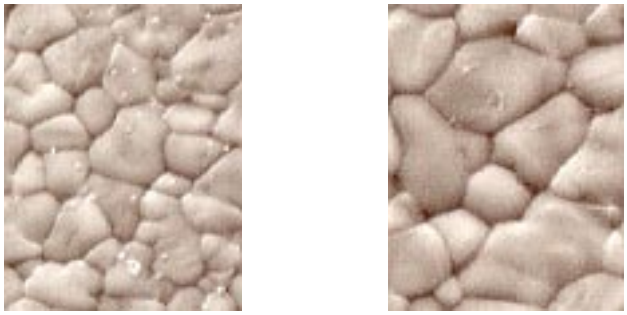

Figure 4-3 CdTe surface SEM photograph (5000X) after isothermal $CdCl_2$ vapor heat treatment at 410˚C (left) and 430˚C (right).

Decoupling the $CdCl_2$ temperature from the reaction temperature shows that reaction temperature has a strong effect in controlling the grain growth, and the two treatment times used for 420/380˚C demonstrates that the grain growth is not kinetically limited in the time spans examined. Sulfur content in CdTe is constant for fixed $CdCl_2$ concentration at reaction temperatures above 380˚C but increased to ~1% by increasing the $CdCl_2$ concentration with $T(CdCl_2)$=450˚C. In general, the recrystallization reduced the (111) preferred orientation from the as-deposited condition.

Repeating the isothermal case at 420˚C but varying the thermal heat-up history of the CdTe/CdS film and the $CdCl_2$ source produced distinct differences in the final structure. Unison heating of the CdTe/CdS and $CdCl_2$ promoted a flat morphology with uniform grain size. The x-ray diffraction results of these films shows extensive diffusion of S diffusion into the CdTe compared to all of the delayed heating reactions (Figure 4-4). The delayed heating method results in a sharp diffraction peak with a small tail extending towards the position of the solubility limit for S in $CdTe_{1-x}S_x$ [405] and is consistent with the low S incorporation shown in Table 4-3. The unison heating produced extended diffusion profiles with alloy layers out to the solubility limit for S in $CdTe_{1-x}S_x$.

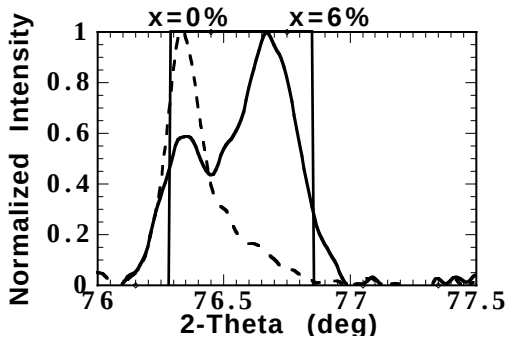

Figure 4-4 High resolution (511) XRD profiles of $CdCl_2$ vapor treated films exhibiting very different degrees of S diffusion.

4.2.1.4.2 Oxygen Effects

Treatment in Ar/O_2 mixtures and at reduced total pressure allowed investigation of the effects of oxygen on film properties and devices. Isothermal reactions at 420˚C for 20 minutes with delayed heating were employed to permit evaluation of the influence of oxygen concentration on the S diffusion. Table 4-4 shows materials data for 2.5 µm CdTe/0.2 µm CdS films treated with $CdCl_2$ vapor under different O_2 concentrations at 420˚C for 20 minutes. All cases were treated in $Ar:O_2$ except the reduced pressure case which was treated under dynamic roughing pump conditions with residual ambient air. Progressive grain growth was obtained with increasing O_2 concentration at 1 atm. total pressure. At very high O_2 concentration, S diffusion is greatly enhanced. The (511) XRD peak profiles for the highest O_2 case resembles the highly alloyed case of Figure 4-4. The optical transmission curves, normalized for reflection, show a progressive shift in location of the CdTe bandedge towards lower energy with increasing oxygen that is consistent with formation of alloy layers with increasing S content (Figure 4-5). The case treated at reduced pressure exhibited no measurable interdiffusion and retained a high degree of (111) preferred orientation. Similar results were obtained on structures with 4.5 µm thick CdTe, which were processed into devices.

Table 4-4. Grain size and x-ray diffraction results for films before and after treatment at 420˚C for 20 min at different pressure and O_2 concentration.

Total P (torr)	$p(O_2)$ (torr)	p(Ar) (torr)	AGS (μm)	a_0 (Å) ±0.001	[S]/ [Te]+[S] (%) (±0.2)	p (111)
as dep	-	-	0.4	6.486	0	4.0
0.04	0.01	0	1.1	6.481	0	3.1
760	0.01	760	1.1	6.477	0.7	0.9
760	190	570	1.4	6.475	0.8	2.4
760	380	380	2.1	6.477	0.7	1.9
760	570	220	2.5	6.462	2.9	1.1

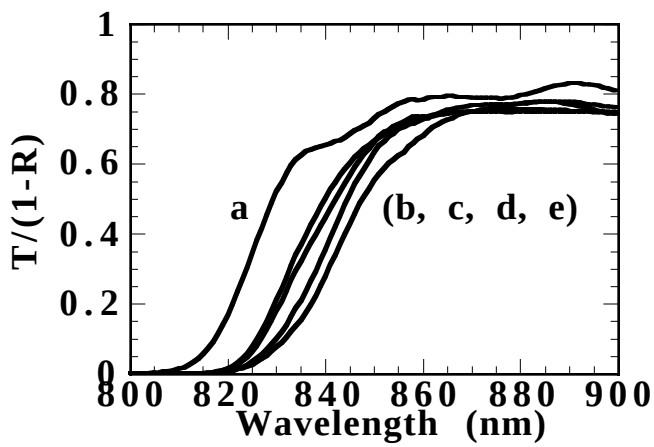

Figure 4-5 Normalized optical transmission curves for CdTe/CdS films of Table 4-4: a) as deposited, b) 0.01 , c) 190, d) 380, and e) 570 mTorr O_2.

4.2.1.5 Device Results

J-V data for samples treated with $CdCl_2$ vapor under various conditions of temperature and atmosphere are shown in Table 4-5. For the isothermal reactions, the device performance is comparable to that obtained by $CdCl_2$:methanol treatment and is optimal at treatment temperatures of 420˚C to 430˚C. We find that the fill factors of devices across each sample are uniform within ±5 rel %.

Table 4-5 Device results for samples treated with $CdCl_2$ vapor. $CdCl_2$ partial pressures are based on Table 4-2.

T_f (˚C)	T_S (˚C)	Atm	P_S (mTorr)	$P(O_2)$ (Torr)	V_{OC} (mV)	J_{SC} (mA/cm^2)	FF (%)	Eff (%)
380	380	Air	1.3	160	740	19.1	57.1	8.1
410	410	Air	5.7	160	763	21.8	58.1	9.7
420	420	Air	9.0	160	815	20.4	67.7	11.3
430	430	Air	14.0	160	786	20.2	71.0	11.3
380	**380**	Air	1.3	160	740	19.1	57.1	8.1
420	**380**	Air	1.3	160	722	20.4	62.9	9.3
450	**380**	Air	1.3	160	734	20.6	62.6	9.5
420	**450**	Air	32.7	160	793	20.9	51.7	8.6
420	420	Ar/O	9.0	**570**	791	23.5	61.8	11.5
420	420	Ar/O	9.0	**0.008**	737	21.9	56.7	9.1
420	420	**Vac**	9.0	0.008	809	21.8	66.5	11.7

At reduced $CdCl_2$ concentration (T=380˚C) but spanning reaction temperature from 380˚C to 450˚C there was little difference in V_{OC}, J_{SC}, and FF with reaction temperature in spite of very different grain size. However, at a reaction temperature of 420˚C, increasing the $CdCl_2$ concentration from 1 mtorr to 33 mtorr improved the V_{OC} to the range obtained in isothermal cases. Thus, for reactions at one atmosphere total pressure of air, isothermal reactions in the range of 420˚C to 430˚C yield comparable performance to the $CdCl_2$:methanol method, but with improved uniformity and reproducibility. This suggests that the beneficial modifications of the $CdCl_2$:air ambient mixture are optimal when the CdTe films are at the temperature required to maintain the $CdCl_2$ at equilibrium in the range from 5 to 10 mtorr.

Oxygen concentration, which was shown to affect interdiffusion and grain growth in the materials, does not appear to play an efficiency limiting or enhancing role in the range explored. The O_2 concentration influences the consumption of CdS and could be used to control that process, either by allowing ultrathin layers to survive processing (low O_2 concentration), or by deliberately promoting consumption (high O_2) to either produce an ultrathin layer from a thicker starting layer or to tailor the CdTe bandgap slightly.

The quantum efficiency spectra of vapor treated devices are similar to those treated by $CdCl_2$:methanol but exhibit reduced interdiffusion, evidenced by the long wavelength cutoff [406]. For devices treated at high O_2 concentration, the short wavelength response for 350-550 nm was higher due to reduction in CdS thickness by the S diffusion.

4.2.1.6 Conclusions

Treatment of CdTe/CdS thin films with $CdCl_2$ vapor can be used for processing of high efficiency devices. Reactions in isothermal mode replicate materials and device results obtained with the commonly used $CdCl_2$:methanol method. The vapor approach produces uniform modification of film properties and chemically clean surfaces resulting in uniform device performance. The materials and device uniformity are not contingent on uniform deposition of $CdCl_2$ on the CdTe

surface. The absence of rinsing and drying steps makes the vapor processing a favorable approach for large area reactions. The extent of grain growth and interdiffusion can be controlled to some extent by the thermal history and oxygen content of the ambient. Greater than 11% conversion efficiency was achieved with films treated in wide range of oxygen partial pressures at 420˚C to 430˚C.

4.2.2 Materials Analysis of $CdCl_2$ treated Films

4.2.2.1 Introduction:

Post-deposition processing of polycrystalline CdS/CdTe solar cells with $CdCl_2$ has been demonstrated to improve cell efficiency by improving the electrical properties of the films for photovoltaic operation [409]. In many cases the treatment also produces significant structural changes which are coupled to the electronic properties of the semiconducting layers and which can impose limits on device performance. Treatment or exposure to $CdCl_2$ is a component of every process for fabricating high efficiency CdTe solar cells, regardless of CdTe film formation temperature. For example, films which are fabricated from sintered powder slurries are processed with $CdCl_2$ additives at temperatures of 600-700˚C to encourage grain growth and film densification [422-425]. Other devices, such as those deposited by physical vapor deposition (PVD) and molecular beam epitaxy, receive a lower temperature treatment to achieve efficiencies in the 11 to 13% range [426, 427]. They are coated with a $CdCl_2$:CH_3OH solution, dried, then heat-treated at ~400˚C. Cells formed by electrochemical deposition receive an analogous treatment where they are synthesized in a plating bath containing Cl ions to produce a Cl-doped CdTe layer and then heat-treated at 400˚C for 30 minutes [428].

Many effects of the $CdCl_2$ processing on the CdTe/CdS layers have been observed but their significance to device operation have not been quantitatively explained. For example, grain growth in both the CdS and CdTe layers is greatly enhanced, while porosity is minimized [409, 422-428], but among the different high efficiency devices represented, a considerable range of grain size, porosity and film orientation is found. Previous work has also established that substantial S diffusion occurs in CdTe films over a wide range of thermal processing temperatures [422-426]. A significant degree of S diffusion has also been noted following 400˚C treatments with $CdCl_2$ in which consistent shifts were observed in the CdTe x-ray diffraction spectra, CdTe optical absorption edge, and the CdTe spectral response cutoff in CdS/CdTe solar cells [406, 409, 426]. In addition, secondary ion mass spectroscopy (SIMS) has shown that the average S content of the CdTe film increases as the distance to the CdS/CdTe interface decreases [429]. During high temperature treatments, T > 500˚C, S diffusion into CdTe is believed to have led to homojunction formation within the S-rich portion of the $CdTe_{1-x}S_x$ layer [424, 425]. These observations are all consistent with the diffusive transport of S into CdTe during $CdCl_2$ processing which reduces the CdS window layer and forms a $CdTe_{1-x}S_x$ layer. Likewise, Te diffusion into CdS produces $CdS_{1-y}Te_y$, which reduces the high energy portion of the device spectral response, resulting in lower current densities. Recrystallization treatments of the CdS layer have been developed which limit the extent of this process [430, 431]. The extent of the CdS consumption establishes a lower limit to the thickness of CdS that can be employed to achieve high efficiency. Control over the effective CdS thickness obtained after processing is thus critical to achieving high current densities while retaining the junction properties of the CdTe/CdS, which controls the open circuit voltage of the device. Loss of the CdS layer will result in formation of a $CdTe_{1-x}S_x$/TCO junction having inferior performance [430].

This paper examines recrystallization and S diffusion in CdTe at ~400˚C through a detailed analysis of CdTe/CdS structures before and after the $CdCl_2$ treatment as a function of treatment time. The treatment temperature and time range used in this work were selected to be in the range

used to make high efficiency devices. Macroscopic and microscopic materials analyses were performed to assess changes in structure and composition of the CdTe layer.

4.2.2.2 Experimental:

4.2.2.2.1 Film Deposition and $CdCl_2$ Treatment

The CdS/CdTe cells were prepared in a superstrate configuration, so that light enters the cell through the transparent conductive oxide (TCO) coated glass superstrate. First, 0.2-0.5 μm of CdS were deposited at 200˚C by evaporation onto indium tin oxide (ITO) coated 7059 glass substrates. CdTe films of several thicknesses, 0.5, 1, 2, and 4 μm, were then evaporated at a growth rate of ~8 Å/s and a substrate temperature of 250˚C on top of the CdS layers. These deposition conditions yielded uniform single phase CdTe films. For transmission electron microscopy (TEM), samples with 2 μm CdTe on 0.5 μm CdS were deposited on polished Si wafers coated with ITO. To ensure that the CdTe/CdS deposited on this substrate yielded comparable electrical performance to the standard cells, a semi-transparent Au layer was used as the contact to CdTe to allow backwall current-voltage measurements to be made. Comparable backwall performance was obtained from the two device structures.

The CdTe/CdS/ITO/7059 samples were coated with 0.8 μm of solid $CdCl_2$ by placing 1 drop per cm^2 of 1% (wt) $CdCl_2$:CH_3OH solution on the top surface of the CdTe film, then evaporating the CH_3OH in a drying oven at 85˚C. During the subsequent air heat-treatment, the samples were held at 415˚C for either 10 or 30 minutes. Thermal transients were minimized by rapid introduction and withdrawal of the samples from the hot zone of the furnace tube. The heat-treatment step was followed by a rinse in deionized water to remove most of the residual $CdCl_2$ coating.

4.2.2.2.2 Microscopy Measurements

The CdTe grain sizes were determined using the method of Heyn [432] from the top surface of the CdTe film and from polished 90 degree sample cross-sections using scanning electron microscopy (SEM). The CdTe grains were clearly distinguishable on the top surface of the samples once they had been rinsed. Polished and etched 90 degree cross-sections were prepared by vacuum impregnating in epoxy, polishing with 0.05 μm alumina grit, then rinsing in hot water.

The CdTe grain boundaries in the polished samples were revealed by first polishing in a 0.0125% (wt) Br_2:CH_3OH solution and then reacting in a 0.1M CuCl/deionized water solution (adjusted to pH=2.25 through addition of HCl) at 65˚C for 30 to 60 seconds. The reaction, CdTe + 2CuCl -> $CdCl_2$ + Cu_2Te, occurs preferentially along grain boundaries. To reveal the grain boundaries, the $Cu_{2-x}Te$ was etched in a 0.2M KCN/water solution at 65˚C for 30 seconds. After each step, the samples were rinsed with room temperature, deionized water and dried.

TEM and energy dispersive x-ray spectroscopy (EDS) was used to examine the cross-sectional grain structure and composition on a CdTe/CdS/ITO/Si sample before and after heat treatment with $CdCl_2$ [433].

4.2.2.2.3 X-ray Diffraction Measurements

The x-ray diffraction (XRD) patterns of the CdTe films were generated using a computer controlled Philips/Norelco diffractometer with Bragg-Bretano focusing geometry and CuK_a radiation. Wide angle 2q scans from 20 to 80 degrees taken at 0.05 degree steps were used to identify the phases present in the samples. The Rachinger correction [435] was used to remove a_2 components for lattice parameter determination and peak profile examination. Errors in peak centrum location

associated with specimen placement and geometry were corrected using the function of Nelson, Riley, Sinclair, and Taylor (NRST), so that the CdTe film lattice parameters could be precisely determined [435-437]. The sulfur content, x, of the $CdTe_{1-x}S_x$ film was determined quantitatively from the lattice parameters by assuming a Vegard's relation:

$$x = 1.508(6.481-a)$$

Equation 4-1

where a is the lattice parameter of the sample.

The degree of preferred orientation in the films was calculated from the a_1 peak intensities of the broad scans using the method of Harris for polycrystalline fiber texture analysis [418]. For the {111} reflection, the orientation parameter, p(111), is defined:

$$p(111) = \frac{N\left[I(111)/I_0(111)\right]}{\left[\sum I(hkl)/I_0(hkl)\right]}$$

Equation 4-2

where N is the number of peaks in the region considered, I(hkl) is the measured intensity of peak (hkl), and I_0(hkl) is the relative intensity of the corresponding peak from a powder reference. For p(111) = N, all the grains of the films are oriented in the <111> direction normal to the substrate, while p(111) = 1 indicates random grain orientation, and p(111) < 1 indicates preferred orientation along an axis other than <111>.

Diffraction scans at 0.01 degree steps were acquired at constant counts per step to obtain constant signal to noise ratio from sample to sample for individual peak profile determination. The peak profiles were assumed to represent the entire sample alloy composition range resulting from diffusion of S into CdTe. To ensure the validity of this assumption, primary and diffracted beam attenuation, which increases surface selectivity, was minimized by using samples less than 3 μm thick. One film was mechanically separated from the TCO/glass and remeasured from the CdS side, yielding the same diffraction profile. To obtain adequate angular resolution, higher order peaks such as the (422), (511) and the (531) were measured. The extent of S diffusion into the grains was shown to be independent of the grain orientation with respect to the substrate surface by examining all (hkl) peak profiles on a single sample. Profiles exhibiting high symmetry, and therefore low diffusion tails, were fit to a Pearson VII function [438] to determine the full width at half maximum (FWHM) for comparison with the diffractometer instrument function. In cases of high asymmetry, Fourier deconvolution of the diffractometer instrument function was performed to establish the limits of compositional broadening.

4.2.2.2.4 Optical Absorption Measurements

Optical transmission, T(λ), and reflection, R(λ), of the CdTe/CdS/ITO/glass structures were measured on a Perkin-Elmer Lambda 9 spectrophotometer and were transformed to an effective absorption coefficient, $\alpha_{eff}(\lambda)$ to allow comparison of the absorption edge location after the various treatments. For this, the effective absorption coefficient of the structure was determined by:

$$\alpha_{eff}(\lambda) = \frac{Ln\left[\frac{T(\lambda)}{1-R(\lambda)}\right]}{d}$$

Equation 4-3

where d is the thickness. Plots of a α_{eff}^2 versus energy were used to determine relative shifts in the absorption edge due to the alloying of CdTe and CdS over a sufficient film thickness to influence the overall absorption. The S content of the absorbing layer was estimated by comparison of the shift of the absorption edge with that reported for kinetically limited or metastable $CdTe_{1-x}S_x$ thin films [405, 439] in which the CdTe bandgap, E_g, is reduced due to formation of $CdTe_{1-x}S_x$ alloys from x=0 to 1 according to:

$$E_g(x) = 1.74x^2 - 1.01x + 1.51 \text{ [436].}$$

Equation 4-4

Equilibration of alloy films at ~400°C leads to a miscibility gap from x=5.8% to x=97% but with similar E_g versus x dependence over the alloy existence region.

4.2.2.3 Results:

4.2.2.3.1 Microscopy

As-deposited films have lateral grain size of ~0.1-0.25 μm depending on film thickness. Films heat treated at 415˚C without $CdCl_2$ for up to 30 minutes have similar structure to as-deposited films, with little observable change in grain size or morphology. However, substantial grain growth occurs for samples coated with $CdCl_2$ (Table 4-6). Figure 4-6 (a-i) shows SEM top surface micrographs of 0.5, 1, and 2 μm thick CdTe films for as-deposited (a-c) and $CdCl_2$ treated at 415˚C for 10 minutes (d-f) and 30 minutes (g-i). For the different CdTe film thicknesses there is a trend toward larger final grain sizes with thicker CdTe films and with longer heat treatment times, although for the 2 μm thick films, the average grain size is the same after 10 and 30 minutes of treatment (Table 4-6). After 30 minutes of treatment there are no detectable sub-micron grains, and the grain boundaries meet at 120˚ angles, as expected for a film in equilibrium [440].

Table 4-6. Tabulated values of grain size, orientation parameter, lattice parameter, and (111) peak intensity for CdTe powder and for CdTe films in 2 μm CdTe/0.5 μm CdS/ITO/glass structures.

Sample	Condition	Average Grain Size (μm)	p(111)	I(111) (counts)	a_0 (Å)	(511) FWHM (deg)
Powder	-	NA	1.0	NA	6.481	NA
Film	As Deposited	0.2	4.0	8849	6.489	0.248
Film	10', 30' and 60' HT no $CdCl_2$	0.2	2.3	4908	6.480	0.140
Film	10' HT with $CdCl_2$	1.3	0.8	5823	6.481	0.140
Film	30' HT with $CdCl_2$	1.3	0.9	3004	6.460	>0.40

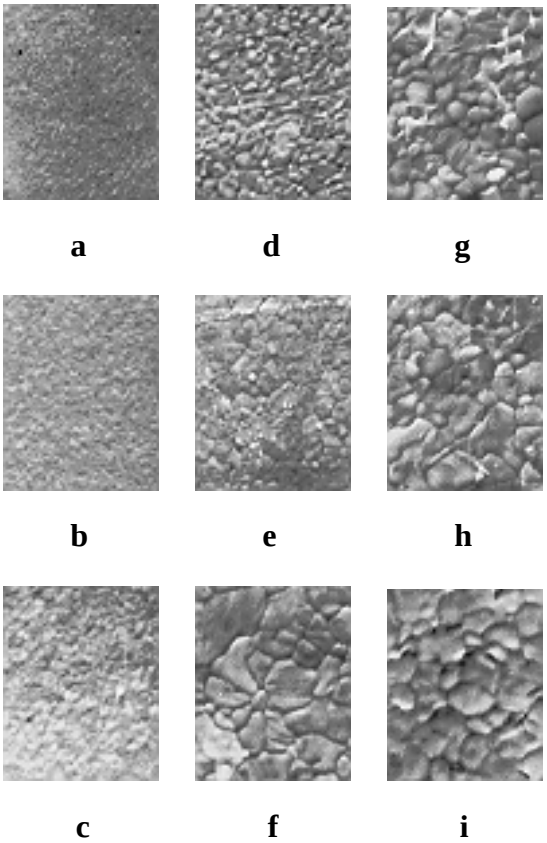

Figure 4-6 SEM top surface micrographs (x 5000) of 0.5, 1, and 2 μm CdTe/0.5 μm CdS/ITO/glass structure in as-deposited condition (a-c); after heat treatment at 415˚C for 10 minutes with $CdCl_2$ (d-f); and after heat treatment at 415˚C for 30 minutes with $CdCl_2$ (g-i).

Cross-section SEM micrographs in conjunction with top surface micrographs show that the increase in grain dimension extends down to the CdTe/CdS interface as shown in Figure 4-7 for 4.5 μm and 2.0 μm thick CdTe samples. The micrographs in Figure 4-7 demonstrate that the coalesced CdTe grains after $CdCl_2$ heat-treatment are at least as wide as they are deep. This is quite different from the as-deposited microstructures, which are difficult to analyze by SEM analysis, since the grain sizes are less than 250 nm.

a b

Figure 4-7 SEM cross-section micrographs (x 5000) of 2 μm and 4 μm CdTe samples after heat treatment at 415˚C for 30 minutes with $CdCl_2$.

Cross-section TEM analysis was carried out on as-deposited 2 μm CdTe/0.5 μm CdS samples and the same samples $CdCl_2$ treated at 415˚C for 30 minutes. The micrographs of the CdTe/CdS/ITO/Si cross-sections suggest that the as-deposited CdTe grains are epitaxial with the underlying CdS grains and are highly faulted and columnar (Figure 4-8). Spot TEM/EDS analysis showed no evidence of S or Te interdiffusion in the as-deposited films. Selected area electron diffraction of the individual layers showed that the CdTe film is predominantly cubic, while the CdS film contains a mixture of cubic and hexagonal phases. High resolution lattice imaging confirmed that the CdTe grains are epitaxially related to the CdS grains[433]. Recrystallization of the as-deposited film is thus energetically favored, since it will reduce the strain energy within the CdTe layer arising from the ~10% lattice mismatch between the CdS (001) and the CdTe (111) planes. After heat treatment with $CdCl_2$, TEM imaging (Figure 4-9) shows substantial grain growth in both layers with little or no epitaxial coordination between the CdS and the CdTe. The TEM micrographs show thermal grooving at the surface of the CdTe near the grain boundaries and independent restructuring of the CdS and CdTe films, resulting from reduction in the interfacial energy. Selected area EDS measurements indicated S and Te interdiffusion across the interface after treatment.

Figure 4-8. TEM cross-section micrograph of 2 μm CdTe/0.5 μm CdS/ITO/Si in as-deposited condition.

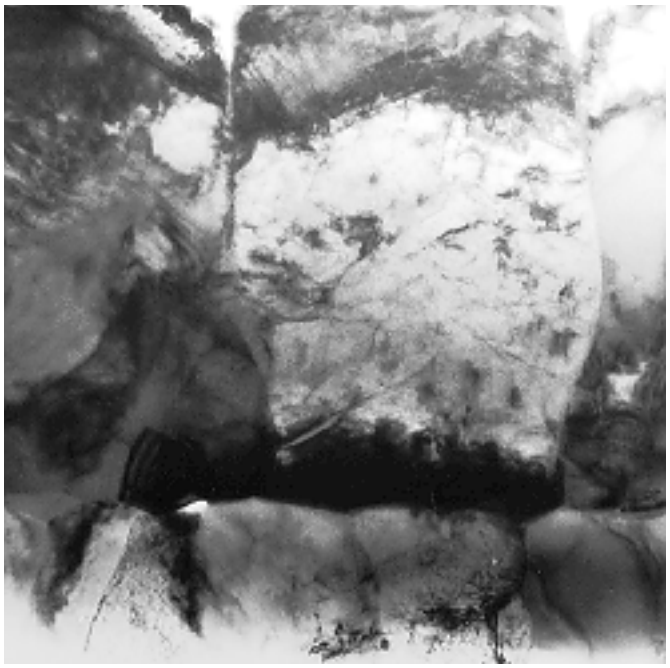

Figure 4-9 TEM cross-section micrograph of 2 μm CdTe/0.5 μm CdS/ITO/Si after heat treatment at 415˚C for 30 minutes with $CdCl_2$.

4.2.2.3.2 Wide Angle X-Ray Diffraction Scans

Wide angle x-ray diffraction scans were made on all samples: as deposited, treated without $CdCl_2$, treated with $CdCl_2$ at 415˚C for 10 and 30 minutes. The XRD scans show that recrystallization of the CdTe film occurs during heat treatment with or without $CdCl_2$. Figure 4-10 specifically compares wide angle scans of an as-deposited sample to two samples cut from the same piece and treated for 10 minutes at 415˚C in air. One of the samples was coated with $CdCl_2$ prior to the heat treatment. The as-deposited film shows a very strong {111} texture with $p(111) = 4$. Heat-treatment at 415˚C for 10, 30, or 60 minutes in the absence of $CdCl_2$ produces a modest degree of sharpening of the individual peaks, and a reduction of preferred orientation to $p(111) = 2.3$. Heat-treatment of $CdCl_2$-coated samples at 415˚C for 10 minutes, however, produces near-random orientation of the grains, with $p(111) < 2$. The samples treated with $CdCl_2$ exhibit additional peaks in the patterns due to residual $CdCl_2$ phases on the CdTe surface after treatment.

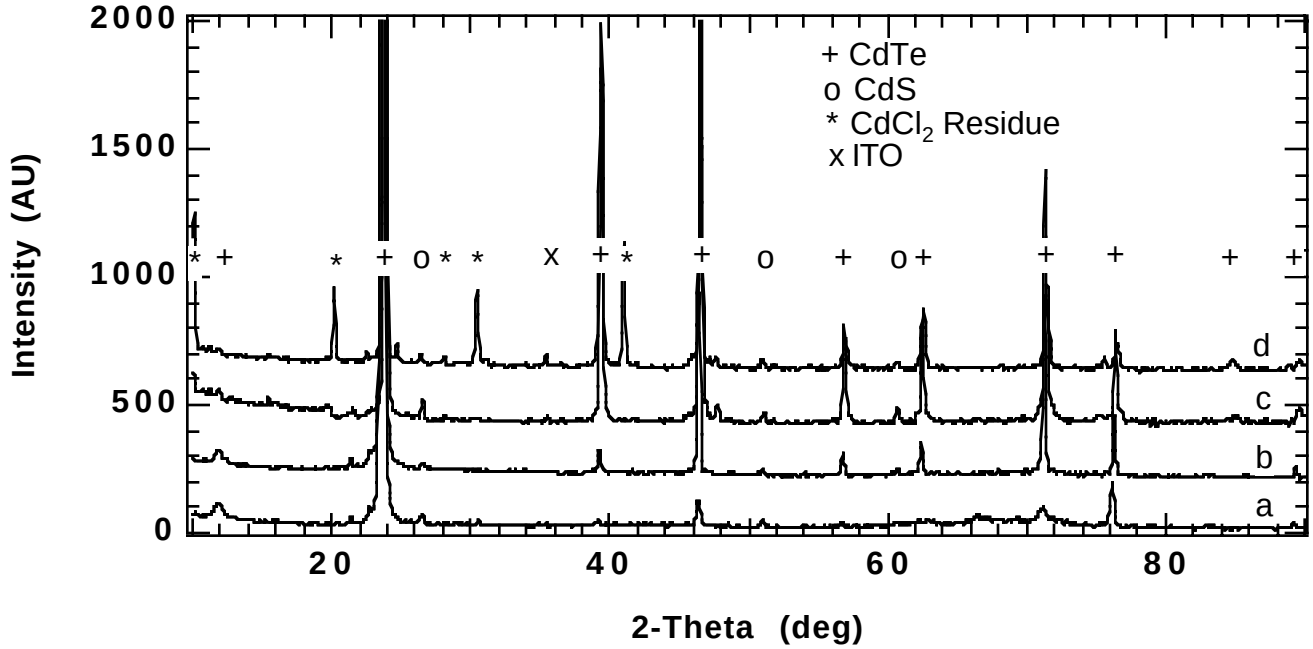

Figure 4-10 Wide angle XRD scans of 2 μm CdTe/0.5 μm CdS/ITO/glass structure in as-deposited condition (a), after heat treatment at 415˚C for 10 minutes with no $CdCl_2$ (b), after heat treatment at 415˚C for 10 minutes with $CdCl_2$ (c) and after heat treatment at 415˚C for 30 minutes with $CdCl_2$.

Heat treatment without $CdCl_2$ shifted all the diffraction peaks slightly towards higher angle, while treatment with $CdCl_2$ shifted and broadened the diffraction peaks towards higher angle. Table 4-6 summarizes the changes in grain size, orientation parameter, precision lattice parameter, and FWHM obtained with and without $CdCl_2$ during heat treatment. The as-deposited films appear to be strained, with lattice parameter greater than expected for CdTe. The increase in a_o along the <hkl> growth axis can be explained by a compressive stress perpendicular to the growth axis, i.e., in the growth plane. The TEM results described above suggest that the heteroepitaxial nature of the CdTe-CdS films can account for strain in the as-deposited films given the ~10% lattice mismatch between atoms in the CdS (001) and CdTe (111) planes. Heat treatment without $CdCl_2$ relieves the strain, which produces the observed reorientation and shift in a_o to that expected for pure CdTe. Consistent with prior work, [425, 428] the heat treatment with $CdCl_2$ shifts the centrum of the CdTe peaks toward smaller lattice parameter. This is explained by the diffusion of sulfur into CdTe to form a $CdTe_{1-x}S_x$ solid solution, since S substitutes onto Te sites in the CdTe lattice and has a smaller atomic radius than Te which reduces the interatomic bond length in the molecule.

4.2.2.3.3 Narrow Angle X-ray Diffraction Scans

High resolution scans of all (hkl) diffraction lines show the same profile, indicating that the CdS-CdTe mixing process is independent of crystallographic direction. Analysis of the (511) CdTe diffraction peaks before and after $CdCl_2$ processing were made to illustrate the strain relief and compositional variations promoted by the $CdCl_2$ processing. Figure 4-11 shows the (511) peak profile of a 1 μm thick CdTe film in the as-deposited state and after 10 and 30 minute $CdCl_2$ heat-treatments at 415˚C. The evolution of the profile indicates either a strain state or compositional inhomogeneity in the CdTe film. Our subsequent analysis is based on the latter assumption, given the supporting evidence of the TEM/EDS and SIMS measurements.

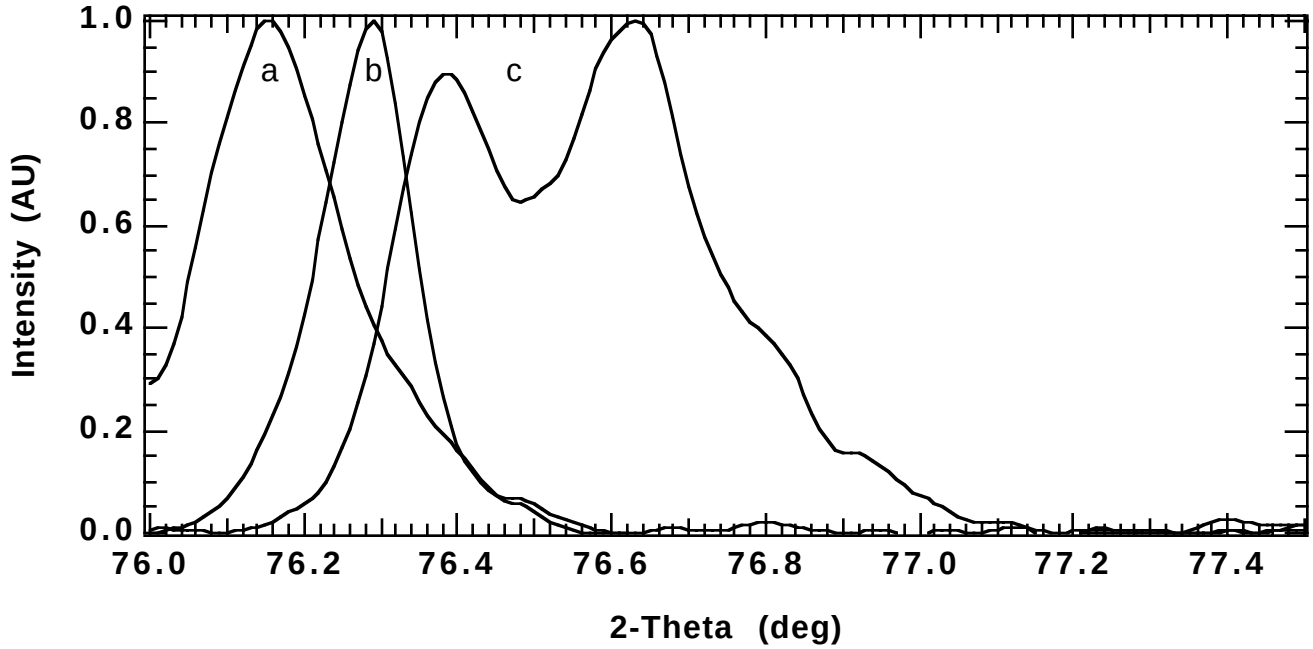

Figure 4-11 XRD (511) profile of 2 μm CdTe/0.5 μm CdS/ITO/glass structure in as-deposited condition (a), after heat treatment at 415˚C for 10 minutes with $CdCl_2$ (b), after heat treatment at 415˚C for 30 minutes with $CdCl_2$ (c).

In Figure 4-11, the centrum of the as-deposited (511) peak profile again has larger d-spacing than expected for pure, unstrained CdTe. The FWHM of the (511) peak is approximately twice that of the diffractometer instrument function. After 10, 30 and 60 minutes of treatment without $CdCl_2$ and 10 minutes with $CdCl_2$ the peak shifted to d-spacing expected for pure CdTe and sharpened to the value obtained for the diffractometer instrument function. Grain coalesence reduced small-particle scattering and relieved the strain which sharpened the peak and shifted the lattice parameter. After 30 minutes of treatment with $CdCl_2$ the peak profile is a doublet having a significant tail extending towards lower d-spacing and lattice parameter.

Fourier deconvolution of the diffractometer instrument function from this profile indicates two strong maxima centered at a_0 = 6.478 Å and a_0 = 6.459 Å, corresponding to compositions of x= 0.5% and x= 3.3%, respectively in $CdTe_{1-x}S_x$. The high angle tail extends to the solubility limit found for S in CdTe [405, 406]. Chemical removal of the top micron of film eliminated the high a_0 component of the diffraction profile so the low S portion of the film was removed. Thus, the S-enriched portion lies in the region of the structure closest to the CdS-CdTe interface. The resulting profile is similar to the profiles obtained from thinner CdTe samples treated under exactly the same conditions as in Figure 4-11. This implies that the compositional distribution with depth is obtained that is independent of the total CdTe thickness and suggests a rapid diffusion process near the CdS-CdTe interface. Thus, treatment with $CdCl_2$ results in CdS-CdTe mixing that cannot be accounted for by a simple single step diffusion process. In curves b and c of Figure 4-12, for 1.0 μm and 0.5 μm thick CdTe films, the primary peak has shifted to the lower lattice parameter, indicating conversion of most of the film to $CdTe_{1-x}S_x$ with x = ~5%. In a 1 μm CdTe film, this corresponds to an equivalent CdS film thickness of ~40 nm that is consumed during the processing.

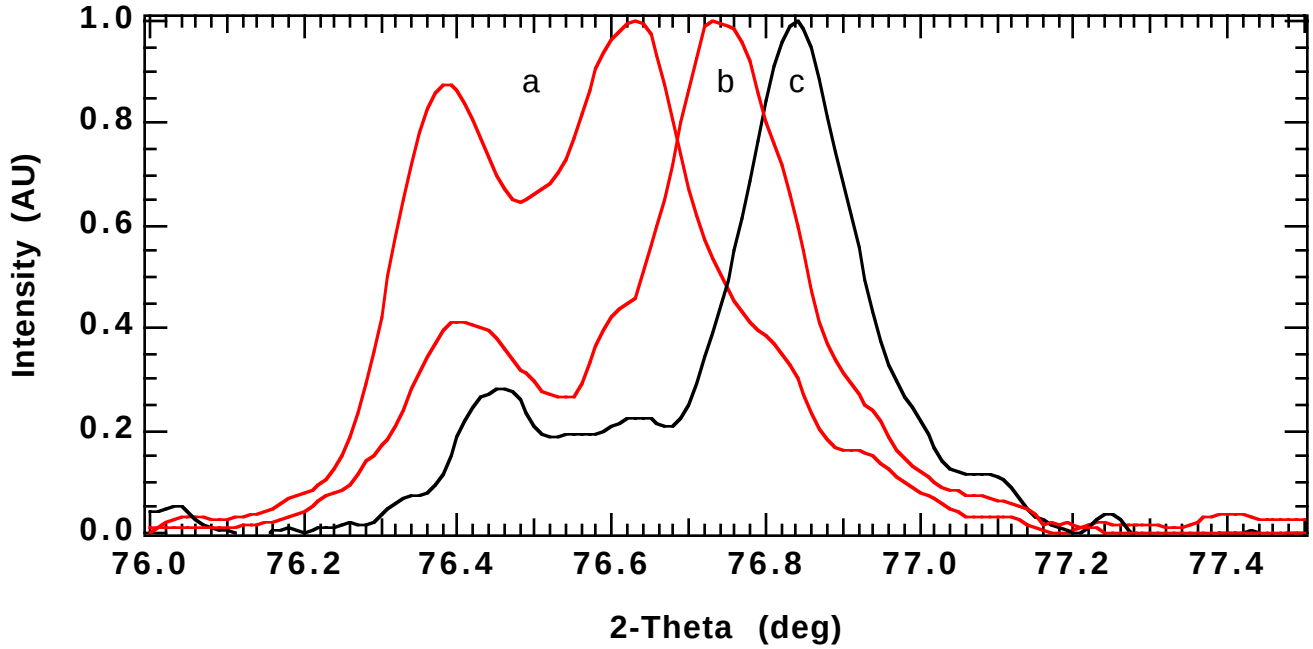

Figure 4-12 XRD (511) profile after heat treatment at 415˚C for 30 minutes with $CdCl_2$ of 2 μm CdTe/0.5 μm CdS/ITO/glass structure (a), 1 μm CdTe/0.5 μm CdS/ITO/glass structure (b), and 0.5 μm CdTe/0.5 μm CdS/ITO/glass structure (c).

4.2.2.3.4 Optical Absorption Measurements

A plot of the square of the absorption coefficient versus photon energy is shown in Figure 4-13 for the 2 μm CdTe/0.5 μm CdS samples of Table 4-6. All samples exhibit similar absorption profiles and the energy shifts caused by the different treatments are listed in Table 4-7.

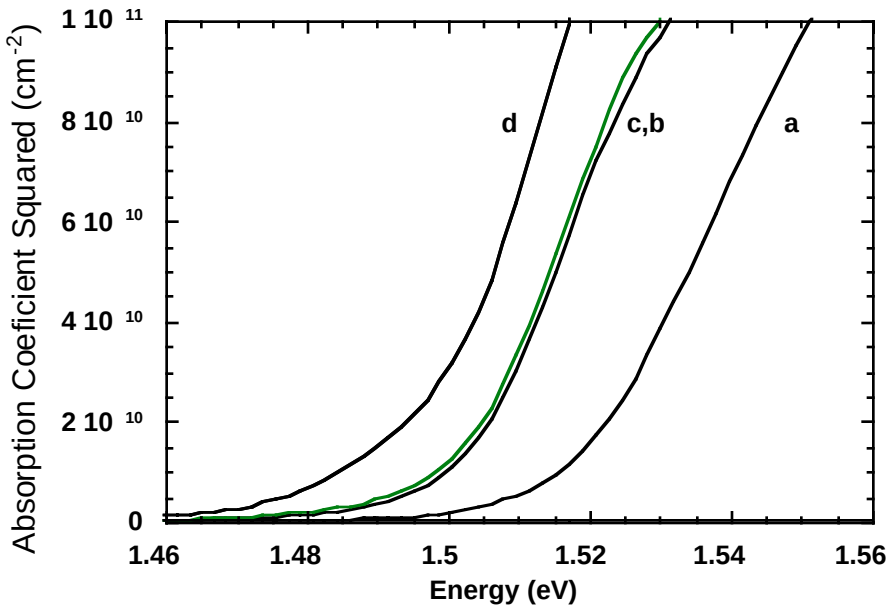

Figure 4-13 Absorption coefficient squared versus energy for 2 μm CdTe/0.5 μm CdS/ITO/glass structure in as-deposited condition (a), after heat treatment at 415˚C for 10 minutes with no $CdCl_2$ (b), heat treatment at 415˚C for 10 minutes with $CdCl_2$ (c), and heat treatment at 415˚C for 30 minutes with $CdCl_2$ (d).

Table 4-7. Tabulated values of relative energy shifts from the as-deposited film at $a^2 = 5 \times 10^{10}$ cm^{-2} in Figure 4-13 and the corresponding S content.

Sample	Condition	ΔE (meV)	% S
a	As Deposited	0	0
b	10', 30' and 60' HT no $CdCl_2$	19	1.95
c	10' HT with $CdCl_2$	20	2.05
d	30' HT with $CdCl_2$	28	2.95

The samples treated for 10, 30 and 60 minutes without $CdCl_2$ and 10 minutes with $CdCl_2$ exhibited the same reductions in the energy of the absorption edge with formation of a $CdTe_{1-x}S_x$ layer containing ~2 % S. After treatment for 30 minutes with $CdCl_2$, however, the composition of the lowest bandgap absorbing layer corresponds to

$CdTe_{1-x}S_x$ containing ~3% S. At first glance, these compositions do not seem to be supported by the diffraction data, but the diffraction data is least sensitive to thin layers near the interface, while the optical data is most sensitive to highly absorbing layers of low bandgap, as expected near the interface. Thus, in the region of the interface, treatment at 400˚C with or without $CdCl_2$ produces some intermixing of CdTe and CdS. This mixing is the primary mechanism for relieving elastic strain in as-deposited samples. For the sample treated with $CdCl_2$ for 30 minutes, the optical measurements indicate the presence of a layer with 3% S while the diffraction data consistently exhibits a maximum at ~3% but tails that extend to 5-6% S, at the solubility limit for S in CdTe [405, 406]. It is speculated that the higher S content regions do not form a continuous film of sufficient thickness to control the optical properties in the plane parallel to the interface. Thus, the higher S content regions (3-6% S) may exist along grain boundaries or other defects.

4.2.2.4 Conclusions:

As-deposited evaporated CdTe/CdS thin film structures consist of single phase columnar CdTe grains that are pseudo-epitaxially oriented on mixed cubic and hexagonal phase CdS films. The CdTe film is highly strained due to lattice mismatch and is free of sulfur.

Heat treatment of the structures at 415˚C without $CdCl_2$ produces little or no detectable grain growth but relaxes interfacial strain due to a small amount of interfacial CdTe-CdS mixing. The treatment also induces some randomization of the CdTe film orientation with respect to the <111> axis.

Heat treatment with $CdCl_2$, needed to produce high efficiency devices from the evaporated materials, induces dramatic grain growth of both the CdTe and CdS layers, reduces surface and interfacial energy, promotes significant CdS-CdTe interdiffusion, and randomizes the CdTe film orientation. The recrystallization occurs in a time frame of ~10 minutes at 415˚C, while interdiffusion is progressive up to 30 minutes and may involve more than one transport process to account for the doublet diffraction peak profiles observed. Further work is necessary to identify the mixing processes and their dependence on $CdCl_2$ concentration, reaction temperature and treatment time. The region near the original CdS-CdTe interface consists of a $CdTe_{1-x}S_x$ alloy with x^a 5%, which is the equilibrium solubility limit for S in CdTe. The extensive alloying forms a non-uniform $CdTe_{1-x}S_x$ layer and consumes a significant quantity of CdS from the device. This establishes a lower limit to the CdS film thickness that can be employed while still retaining a discreet CdS coating on the TCO.

4.3 CdTe-CdS ALLOYS AND DEVICES

4.3.1 INTRODUCTION

Interdiffusion between the window and absorber layer materials occurring during the processing of CdS/CdTe-based solar cells has been widely reported [409, 441-444]. The diffusion of Te into CdS results in the alloy, $CdS_{1-y}Te_y$, which features a wurtzite structure and a lower band gap than CdS. Thus, the diffusion of Te into the window layer has been observed to decrease the J_{SC} of the device [430, 442]. Similarly, the diffusion of S into CdTe results in the zincblende structured alloy, $CdTe_{1-x}S_x$, which features a lower band gap than CdTe. The effect of the formation of this alloy on device performance is difficult to estimate. A correlation between higher V_{OC} and enhanced interdiffusion has been claimed by at least one group [444]. The lower band gap could, conceivably, result in a lower V_{OC} and higher J_{SC}, but the better lattice match and corresponding reduction of interface states could also raise V_{OC} by lowering J_0. The possible effects of a difference in the native defect density between CdTe and the $CdTe_{1-x}S_x$ is also open for speculation.

As a further complication, sulfur diffuses into the CdTe during processing more quickly along grain boundaries than into the bulk of the grains [413]. This process results in a spatially non-uniform composition in the absorber layer conceivably resulting in two or three dimensional effects, and in a non-uniform consumption of the CdS window layer possibly resulting in pinholes.

The significance of the interdiffusion process will clearly depend on the composition of the alloys formed . If the diffusion process were allowed to continue long enough, the window layer would eventually contain the solubility limit of Te in CdS, and, provided that the CdS layer was sufficiently thick, the absorber layer would contain the solubility limited amount of S in CdTe.

These solubility limits have previously been measured only at temperatures no lower than 650°C [445].

In the work presented here, the solubility limits of S in CdTe and Te in CdS at typical temperatures used for device processing are derived by growing alloyed thin films with compositions within the miscibility gap and heat treating them in the presence of $CdCl_2$. Conventional CdTe/CdS devices are then compared to devices where the alloy composition of the absorber layer is uniformly at the solubility limit of S in CdTe, and to CdTe/ITO devices which contain no sulfur in the absorber layer.

4.3.2 EXPERIMENT

4.3.2.1 Alloyed Film Fabrication and Characterization

Thin films of $CdTe_{1-x}S_x$ were grown on glass, In_2O_3:Sn (ITO)/glass, and CdS/ITO/glass substrates by co-evaporation of CdS and CdTe at substrate temperatures of 200 and 250°C. Energy dispersive spectroscopy (EDS) was used to measure the overall atomic composition of the films. X-ray diffraction (XRD) analysis was used to determine the structures of the phases within the films. The atomic compositions of each phase within the films were estimated by using a Nelson-Riley-Sinclair-Taylor plot to extract a lattice parameter from the XRD peak positions, and then applying Vegard's law.

The optical transmission and reflection of the films were measured and used to estimate the absorption constant, a. The linear portion of $(ahn)^2$ verses hn was extrapolated to obtain an optical band gap.

4.3.2.2 Film Treatment

The alloyed films were subjected to one of two $CdCl_2$ heat treatment methods. In the traditional surface method, $CdCl_2$ was deposited directly on the film [409]. In the vapor method, $CdCl_2$ was kept at distance ≈0.1 mm away from the film surface 416]. In both cases, the $CdCl_2$ and film were heated in air at 415 to 420°C.

4.3.2.3 Device Processing

Conventional CdTe/CdS solar cells were made by vacuum evaporation of ~200 nm CdS and then ~5 µm of CdTe onto ITO/glass substrates. These structures were given a $CdCl_2$ vapor treatment in dry air at 420°C for 20 minutes. Back contacts were made to the devices by the deposition of 100 Å of copper, diffusion of copper into the film by heating at 180°C for 30 minutes in an argon atmosphere, etching away the copper remaining on the surface with a solution of bromine in methanol and then applying graphite paste [446]. Indium solder applied to the ITO served as the front contact.

$CdTe_{1-x}S_x$ /CdS/ITO, $CdTe_{1-x}S_x$/ITO, and CdTe/ITO solar cells were produced in a manor very similar to the conventional CdTe/CdS cells. The $CdTe_{1-x}S_x$ layers were deposited with a sulfur content of x=5 to 6%. The processing conditions used for each of the four device structures compared in this work are given in Table 4-8. The 200°C copper diffusion temperature was found to be critical to obtaining satisfactory $CdTe_{1-x}S_x$/CdS devices. The $CdTe_{1-x}S_x$/CdS devices treated at 180°C typically suffered from low J_{SC}, voltage dependent collection, and blocking contact behavior. For the CdTe/ITO device, a 500 Å thin insulating layer of ITO was deposited on the 20Ω/square ITO substrate prior to CdTe deposition. The use of this layer improved the J_{SC} and

consistency of these devices. The use of an insulating ITO layer with $CdTe_{1-x}S_x$/CdS devices has not yet been explored.

Table 4-8 Device Processing Conditions (CdS thickness, substrate temperature during absorber layer deposition, as-deposited sulfur content, and copper diffusion temperature) and Performance Characteristics.

Device Structure	CdS thick. (Å)	substr. temp. (°C)	x (%)	Cu diff. temp. (°C)	V_{OC} (mV)	J_{SC} (mA/ cm^2)	FF (%)	h (%)	Label in Figs. 4, 5 & 6
CdTe/CdS/ITO	2600	275	0	180	769	20.4	67.6	10.6	(1)
CdTe/i-ITO/ITO	0	275	0	180	482	24.5	55.7	6.6	(2)
$CdTe_{1-x}S_x$/CdS/ITO	1800	250	5	200	787	21.1	64.8	10.8	(3)
$CdTe_{1-x}S_x$/ITO	0	250	5.5	200	336	22.7	36.2	2.8	(4)

4.3.3 RESULTS AND DISCUSSION

4.3.3.1 Properties of As Deposited Films

As-deposited $CdTe_{1-x}S_x$ films grown on ITO/glass and glass substrates were produced with overall atomic compositions ranging from x= 0 to 0.45. XRD analysis revealed that films with $x < 0.3$ were predominately single phase having a zincblende structure. Films with $0.35 < x < 0.45$ contained the wurtzite modification. The composition of the dominant phase in each as-deposited film closely matches the overall composition of the film (see Figure 4-14), even when the overall composition is well within the miscibility gap shown on published pseudo-binary phase diagrams for the CdTe-CdS system. The miscibility gap on these phase diagrams extends from x=0.16 to 0.86 at 650°C [416] and should be even wider at lower temperatures due to the smaller influence of the entropy on the free energy of the system. Therefore, these films demonstrate that single phase material of either structure may be created with compositions within the miscibility gap. The variation of optical band gap with composition was found to agree well with the data of [439].

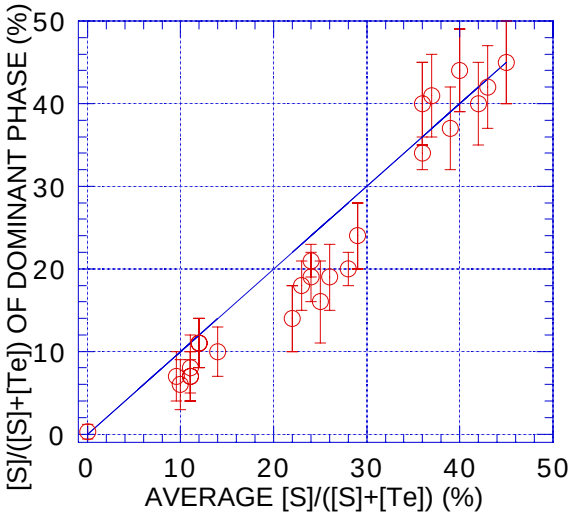

Figure 4-14 For each as-deposited film grown on ITO/glass substrates, the composition of the dominant phase, as determined by XRD analysis, is plotted against the average composition of the film, as measured by EDS. The solid line indicates where the two compositions are equal.

4.3.3.2 Response to $CdCl_2$ Treatment

XRD analysis revealed that heat treatment in the presence of $CdCl_2$ at 415°C caused the films with x>6% to segregate into two phases. The phase segregation process for one film is shown in Figure 4-15. It is felt that the phase distributions of the as-deposited films were either metastable or kinetically controlled, and that heat treatment drove the films towards equilibrium. The rate of phase segregation was affected by the sulfur content of the films and the $CdCl_2$ treatment method, but the end-point composition was not. If the $CdCl_2$ is assumed to only promote the phase segregation process, then the compositions of the two phases after heat treatment may be taken as measurements of the solubility limits of S in CdTe and Te in CdS, respectively. The 415°C solubility limit of S in CdTe is, thus, x'=0.058±0.003, and the solubility limit of Te in CdS is y'=[Te]/([S]+[Te])=0.03±0.01.

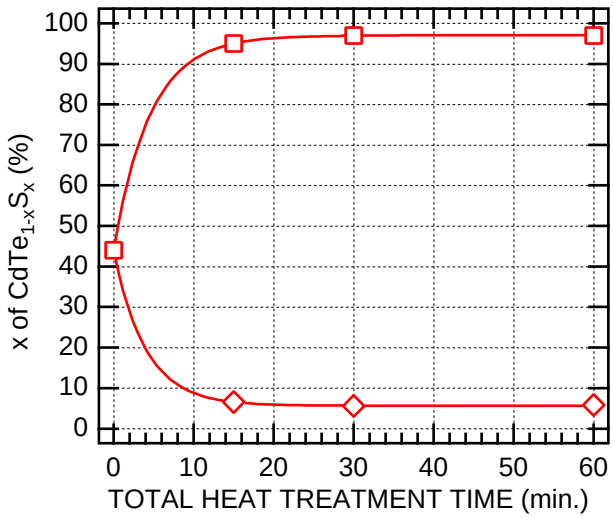

Figure 4-15 Composition of the zincblende structured (diamonds) and wurtzite structured (squares) phases in a film with an average composition of 40.3% as a function of $CdCl_2$ treatment time.

The grain structure of the $CdTe_{1-x}S_x$ films after $CdCl_2$ treatment was found to be quite different than the structure of CdTe films, even when x was less than the solubility limit. A surface layer is suggested by the cross-sectional view shown in Figure 4-16. A preliminary EDS analysis indicates that the surface layer may be richer in sulfur than the bulk. Clearly, the grain restructuring that occurs during $CdCl_2$ treatment is significantly influenced by the presence of sulfur in the film.

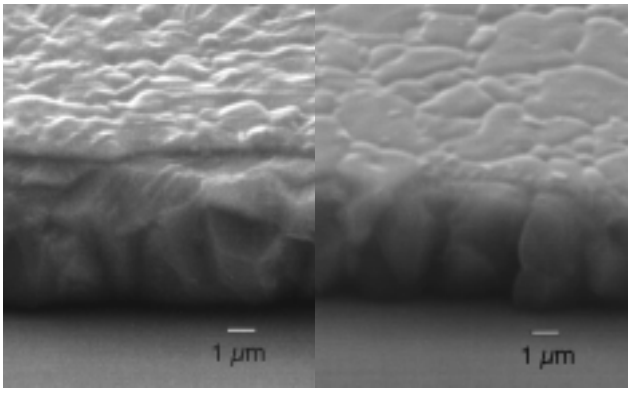

(a) **(b)**

Figure 4-16 Cross-sectional Scanning Electron Micrograph of (a) an alloyed film with a sulfur content [S]/([S]+[Te])=0.05, and (b) a CdTe film. The ~ 5 µm thick films received identical $CdCl_2$ heat treatments.

4.3.3.3 Device Results

As shown in Table 4-8, a $CdTe_{1-x}S_x$/CdS device with efficiency near 11% was obtained. The current-voltage characteristics of this device are comparable to those of the conventional CdTe/CdS device (see Figure 4-17). In comparison, the CdTe/ITO device features a high J_{SC} due to the

absence of absorption from CdS (see Figure 4-18), but suffers from low V_{OC}. The best of the $CdTe_{1-x}S_x$/ITO devices made so far, suffer from even lower V_{OC} and voltage depend collection. It is not yet known whether these problems can be improved by adjusting the processing conditions.

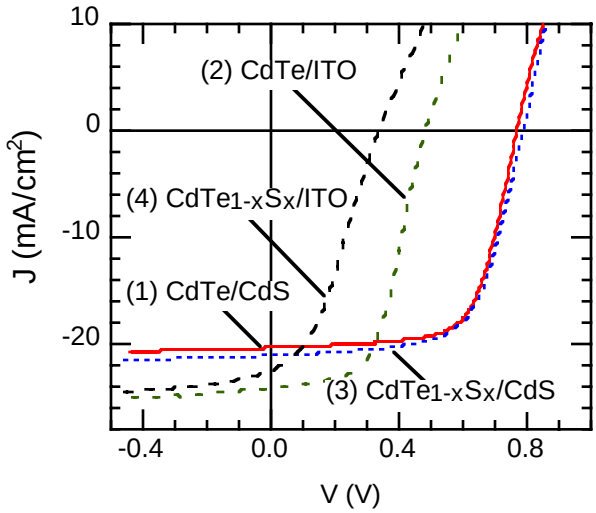

Figure 4-17 Current-voltage characterstics under standard AM1.5 global illumination conditions of the four devices listed in Table 4-8.

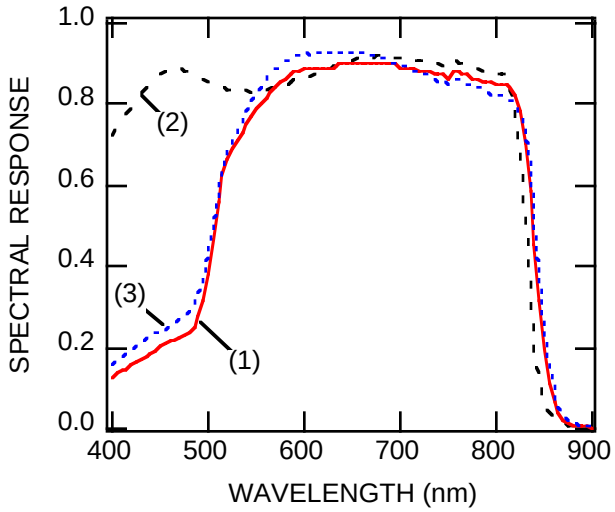

Figure 4-18 The spectral response under light bias of three of the devices listed in Table 4-8: (1) a conventional CdTe/CdS solar cell, (2) a CdTe/ITO solar cell, and (3) a $CdTe_{1-x}S_x$/CdS solar cell.

The similarity of the $CdTe_{1-x}S_x$/CdS device and the conventional CdTe/CdS device is further emphasized by the region of the spectral response near 850 nm where collection drops due to the band edge of the absorber material. That the drop in collection at the band edge of the conventional CdTe/CdS device closely matches the $CdTe_{1-x}S_x$/CdS device rather than the CdTe/ITO device indicates that sulfur content of the conventional device must be near the solubility limit in the region close to the junction where the majority of photons are absorbed. The band edge of the CdTe/ITO

device stands apart from the others because, of the devices studied, it is the only device with a non-alloyed absorber layer after processing.

The physical difference between the $CdTe_{1-x}S_x$/CdS and CdTe/CdS device structures is primarilly the uniformity of the alloy composition in the absorber. The absorber of the $CdTe_{1-x}S_x$/CdS device was deposited with a sulfur content of x=5%. Since this is close to the solubility limit of S in CdTe, little to no increase in the sulfur content due to diffusion of S from the CdS layer was expected to occur during the cell processing. We believe, therefore, that the composition of the absorber layer of these cells is uniformly 5 to 6%. This is in contrast to the sulfur content in the absorber of conventional CdTe/CdS devices which has been found, after processing, to approach 6% near the CdS interface, and be less than 1% throughout the bulk of the material [405].

The difference between the uniformity of the absorber layers is evident only in the long wavelength tail of the spectral response where light penetrates more deeply into photon energy, it is seen that the band edge of the $CdTe_{1-x}S_x$/CdS device is uniformly ~25 mV lower than that of the CdTe/ITO device (see Figure 4-19) which is consistent with the lower band gap of the alloy. While the spectral response of the conventional device matches that of the $CdTe_{1-x}S_x$/CdS device in the high absorption region, at lower energies, where light is absorbed more uniformly though the absorber, the response tends towards that of the CdTe/ITO device. These results indicate that the bulk of absorber contains much less sulfur than the interface region.

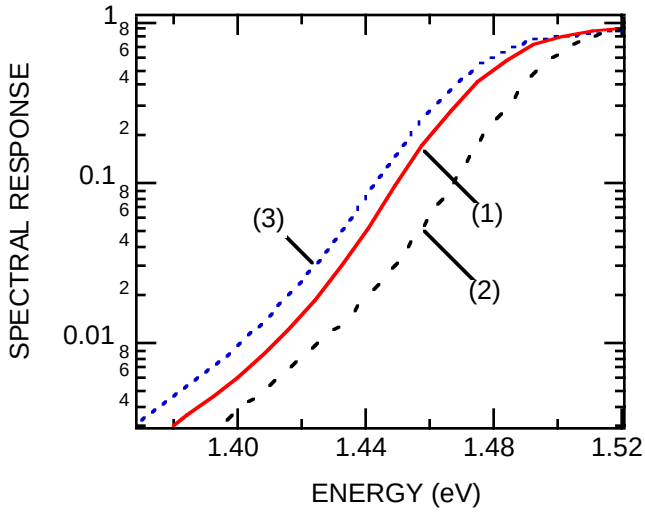

Figure 4-19 Long wavelength edge of the dark spectral response plotted against photon energy of (1) a conventional CdTe/CdS solar cell, (2) a CdTe/ITO solar cell, and (3) a $CdTe_{1-x}S_x$/CdS solar cell.

4.3.4 CONCLUSIONS

Predominately single phase thin films of $CdTe_{1-x}S_x$ have been deposited by vacuum co-evaporation with compositions within the miscibility gap of the CdTe-CdS alloy system. These films phase segregated upon $CdCl_2$ heat treatment allowing a determination of the solubility limits of S in CdTe and Te in CdS. $CdTe_{1-x}S_x$ films with a uniform composition near the solubility limit of S in CdTe were grown on CdS/ITO substrates and processed into devices. The J-V characteristics and spectral response of these devices are very similar to conventional CdTe/CdS devices processed in a similar manner. In other words, the alloy formation due to the diffusion of S that takes place during processing of conventional CdTe/CdS devices results in device behavior very similar to that

of devices with alloy composition at the solubility limit of S in CdTe uniformly throughout the absorber. These results suggest that two or three dimensional effects due to the spatial non-uniformity of alloy composition do not play a significant role in conventional devices with efficiencies up to 11%.

4.4 HCl VAPOR TREATMENT

4.4.1 Introduction

Fabrication of high efficiency CdTe/CdS thin film solar cells using CdTe deposited by non-screenprint or spray methods relies on a post-deposition treatment of the CdTe/CdS structure with $CdCl_2$ to improve the junction properties [410, 411, 447]. The most widely used treatment technique involves coating the CdTe surface with a $CdCl_2$:methanol solution, evaporating the methanol, heating at temperatures near 400˚C, and rinsing the surface. However, this treatment is not amenable to high-throughput large scale processing due to problems associated with uniform application of the $CdCl_2$ coating, removal of post-treatment residues, and safe management of large quantities of the Cd salt. Alternative techniques such as evaporating $CdCl_2$ onto the CdTe [448], or reacting the CdTe/CdS in either $CdCl_2$ vapor [402, 414, 415] or Cl_2 vapor [415] have been shown to be suitable substitutes and are more amenable to large scale processing. Of these, the Cl_2 offers advantages with respect to vapor generation and Cd toxicity. Dilute mixtures of HCl offer another possibility. In this paper we report on the effects of treatment of physical vapor deposited CdTe/CdS structures in HCl vapor as a function of HCl concentration and treatment temperature. The effects on both materials properties and device performance are considered.

4.4.2 Experimental Considerations

There are several practical concerns that must be considered when performing the heat treatment (HT) in HCl. These issues not only played a role in developing the procedures reported herein, but may also be important in evaluating the commercial potential of this process step.

4.4.2.1 Source Gas

Initially the experiments were conducted using HCl gas generated by bubbling Ar through concentrated (25 Mol%) hydrochloric acid and the HCl concentration in the anneal ambient was determined from the integrated gas flow and the amount of HCl measured by titration in an exhaust bubbler. Bubbling Ar through hydrochloric acid led to experimental difficulties related to excessive H_2O vapor and poor control of HCl concentration. The origin of these difficulties is attributed to the fact that the HCl-H_2O system has an azeotrope such that liquid condenses (as on tubing or reactor walls or even the inside of the acid beaker) at a concentration of about 11 Mol%. The vapor in equilibrium with this condensed liquid is approximately 97 Mol% H_2O [449, 450]. In practice, the system displayed considerable hysteresis with respect to the measured HCl concentration. Once HCl had been introduced into the system its was difficult to remove it, and conversely, in freshly cleaned apparatus the HCl concentration was less than expected.

Another concern is the effect of humidity on the HT. From the literature we know that dry HCl is not very reactive and that reactions with dry HCl often take place only in the presence of catalysts whereas hydrogen chloride in water (hydrochloric acid) is an aggressive reagent [449, 450]. For both of these reasons it was decided to change the source gas from Ar bubbled through concentrated hydrochloric acid to dry HCl mixed with Ar. As condensation is to be avoided, at no time should the humidity of the source gas reach a level at which condensation occurs.

4.4.2.2 Oxygen

The effect of O_2 in the ambient HT gas could not be investigated because at T ~400 ˚C, heating in mixed HCl and O_2 produces coatings of solid $CdCl_2$ and Te layers on top of the CdTe surface. Earlier work has shown that Cl_2 reacts with CdTe to form $CdCl_2$ and Te [413]. In practice this reaction appears to dominate any other effect, such as oxygen doping, that might occur during the HT.

4.4.3 Experimental Techniques

4.4.3.1 Sample Preparation

The samples have the superstrate structure of 7059 glass/ITO/CdS/CdTe. ITO was deposited by sputtering to a thickness of ~2000 Å and sheet resistance of ~20 Ω/sq. Both CdS and CdTe were deposited by thermal evaporation with substrate temperatures of 200˚C and 275˚C and film thicknesses of 2200 Å and 5 μm, respectively.

4.4.3.2 Experimental Apparatus

The HCl post-deposition treatment was conducted in an evacuatable tube furnace system. Before each run the furnace was evacuated with a mechanical pump to ~0.1 torr and backfilled with high purity Ar. Two thermocouples were installed in the system, one was used for furnace temperature control and the other for measuring sample temperature. Commercial 5% HCl in Ar from Matheson was used as the HCl source. The concentration of HCl in the reaction chamber was reduced by adding additional Ar.

4.4.3.3 Experimental Parameters

Samples were divided into two groups. One group was used to study the effect of HCl concentrations of 0, 0.5%, 1.6%, 3.0% and 5% during a HT at a temperature of 400˚C for 30 minutes. The second group was used to study the effect of temperatures of 380, 400, 420 and 440˚C with a fixed 5% HCl concentration for 30 minutes.

After the film properties had been measured, back contacts were applied using the "diffused Cu" method [446] and applying carbon paste electrodes. The irregular shape of these electrodes led to ~10% uncertainty in the determination of device area and therefore of the current density.

4.4.4 Characterization

4.4.4.1 Film Morphology and Grain Size

The effects of treatment on the surface morphology and chemical composition were measured by scanning electron microscopy (SEM) and energy dispersive spectroscopy (EDS). The average grain size (AGS) was calculated by dividing the length of a line drawn across the SEM micrograph by the number of intersections with grain boundaries and then dividing by the magnification.

4.4.4.2 Preferred Crystal Orientation

The degree of preferred (111) orientation, p(111), was quantified from x-ray diffraction scans using the method of Harris for polycrystalline fiber texture analysis [418]. For the (111) peak this quantity is:

$$p(111) = \frac{I(111)/I_0(111)}{\frac{1}{N}\sum_{hkl} I(hkl)/I_0(hkl)}$$

Equation 4-5

where N is the number of peaks in the region considered, I(hkl) is the measured intensity of peak hkl, and I_O(hkl) is the relative intensity of the corresponding peak from a powder sample. In this case p(111) = 9 means that the film is completely (111) oriented while p(111) = 1 implies perfectly random distribution.

4.4.4.3 **Optical Measurements**

Transmission and reflection were measured to determine the absorption edge location, which allows shifts in the bandgap, ΔE_g, to be observed. The bandedge is expected to shift due to the formation of the $CdTe_{1-x}S_x$ as a result of interdiffusion near the CdTe/CdS interface. The shift was measured with respect to the absorption of as-deposited CdTe which has been confirmed by XRD measurements of lattice constant to have $x \approx 0$. The value of x was estimated assuming linear variation of E_g over the range 0 to 6% [451]. The shift in bandgap was determined from a plot of the absorption coefficient squared versus energy.

4.4.5 Results And Discussion

Results of the above measurements for films heated at 400 ˚C in various HCl:Ar concentrations are listed in Table 4-9; results for films heated at various temperatures at 5 vol% HCl:Ar are listed in Table 4-10.

Table 4-9 Film parameters vs HCl:Ar concentration (vol%) during a 30 min. HT at 400˚C.

[HCl] (vol%)	AGS ±0.1 (µm)	p(111)	d(111)±0.01 (Å)	ΔE_g (meV)	[S], x (%)
as-dep	0.7	4 - 7	3.76	0	0
0	0.7	2.8	3.76	~5	~0.5
0.5	0.9	1.3	3.75	~10	~1.0
1.6	1.0	1.7	3.74	~15	~1.5
3.0	1.2	2.7	3.73	~15	~1.5
5.0	1.1	1.2	3.74	~15	~1.5

Table 4-10. Film parameters vs temperature during a 30 min. HT in 5 vol% HCl:Ar

Temp (˚C)	AGS ± 0.1 (μm)	p(111)	d(111) ±0.01 (Å)	ΔE_g (meV)	[S], x (%)
380	1.0	1.9	3.76	~10	~1.0
400	1.0	3.2	3.77	~15	~1.5
420	1.2	1.8	3.75	~15	~1.5
440	1.4	0.8	3.75	~20	~2.0

4.4.5.1 **Film Properties**

SEM and EDS analysis pictures show that the surfaces of samples treated in HCl+Ar are clean and without residue.

Thermally evaporated as-deposited CdTe films have an average grain size of ~0.7 μm for 5 μm thick films. Figure 4-20 and Figure 4-21 show the surface structure for films heated in various HCl:Ar concentrations and temperatures. The measured average grain sizes are listed in Table 4-9. HCl in the anneal ambient clearly promotes grain growth; heating without HCl produced no change in average grain size. This confirms that HCl (as $CdCl_2$ does) may work as a flux which breaks down atomic diffusion barriers at grain boundaries and thereby promotes grain growth. The average grain size increases with increasing temperature over the range of 380 to 440˚C, but only in the presence of HCl.

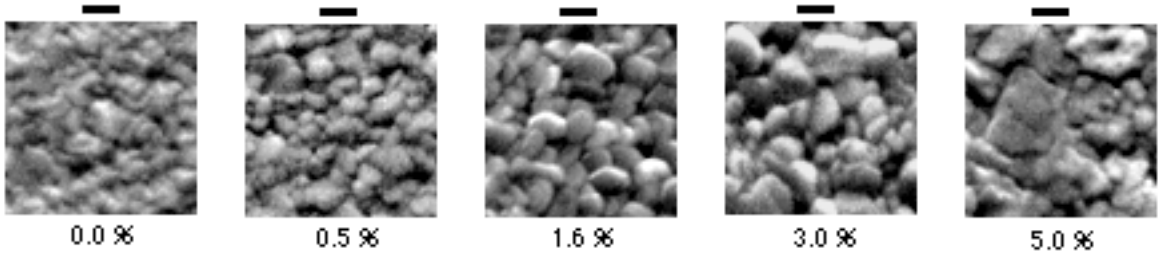

Figure 4-20. SEM photos of the surface of CdTe films heated at 400˚C for 30 minutes at the HCl:Ar concentrations indicated. The scale bar is one micron.

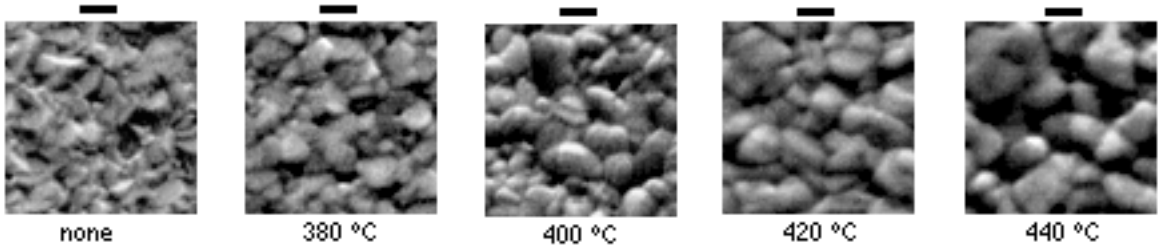

Figure 4-21 SEM photos of the surface of CdTe films heated in 5% HCl for 30 min. at the indicated temperatures. The scale bar is one micron.

It was found that for thermally evaporated as-deposited CdTe films, p(111) is usually in the range of 4 - 7. After post-deposition heat treatment in HCl+Ar for 30 minutes p(111) usually decreases to the range of 1-3. In addition, the data listed in Table 4-9 suggest that for these samples there is also a decrease in the lattice constant.

Plots of the square of the absorption coefficient versus energy are shown in 4-22 and Figure 4-23 for the CdTe/CdS structures treated at 400˚C for 30 minutes at varying HCl:Ar concentration and at various temperatures in 5% HCl:Ar.. With increasing HCl concentration the optical absorption curves indicate a decrease in bandgap. The bandgap shift with HCl concentration suggests that the effect of the HCl reaches the CdTe/CdS interface, perhaps through grain boundaries, and enhances interdiffusion.

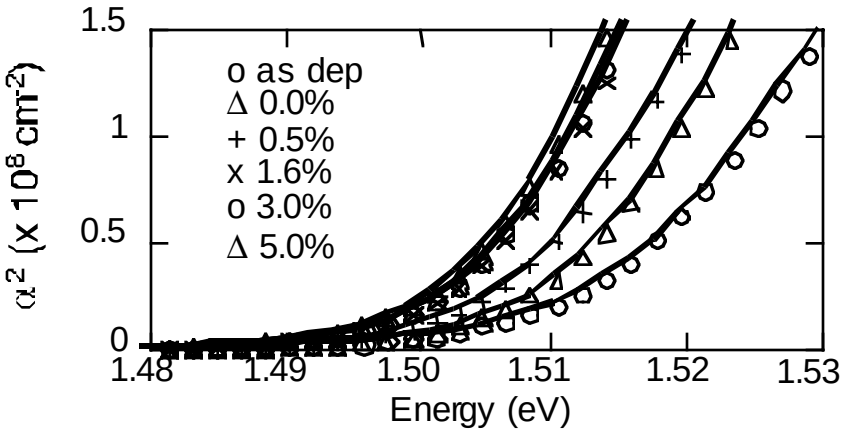

Figure 4-22 Plot of absorption coefficient squared versus energy for CdTe/CdS films treated at 400˚C for 30 minutes at the HCl:Ar concentrations shown.

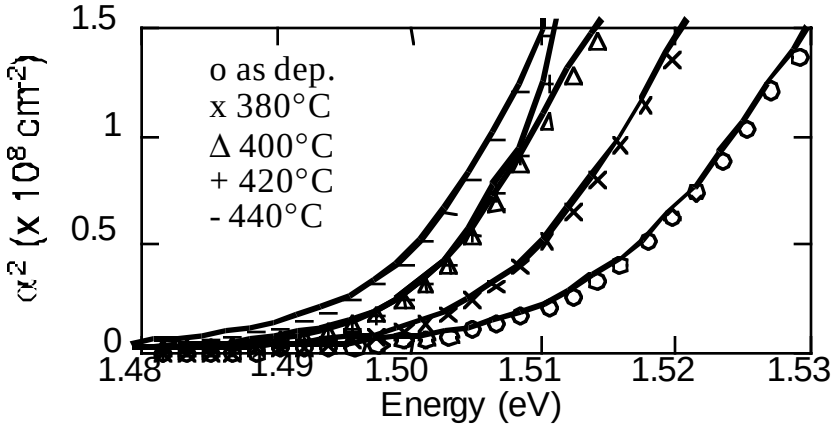

Figure 4-23 Plot of absorption coefficient squared versus energy for CdTe/CdS films treated in 5% HCl:Ar for 30 minutes at the temperatures indicated.

4.4.5.2 Cell Results

The effect of HCl concentration on the dark and light J-V behavior of devices is shown in Figure 4-24, for increasing HCl concentration from 0 to 5%. From the light data we note that carrier collection, as determined from the magnitude and slope of the curve near J_{SC}, improves with HCl

concentration. It is not clear whether increasing concentration above the range included in this study would produce results similar to those obtained using $CdCl_2$ treatments. Figure 4-24 also shows that the light-dark crossover is less severe at the higher HCl concentrations suggesting that conductivity increases with HCl concentration. The mechanism for this is not apparent. In addition, it was noted that hysteresis between forward and reverse voltage sweeps was reduced at higher concentrations as well.

The effects of process temperature variations are summarized qualitatively in Figure 4-25. Changing the temperature of the heat treatment in 5% HCl over the range 380 to 440 ˚C had minimal effect on light or dark J-V behavior. The scatter in data is such that no trends are evident in either the light or dark J-V data. In addition, all of the HCl heat treated devices are characterized by strong light-dark crossover in the first quadrant and poor collection efficiency.

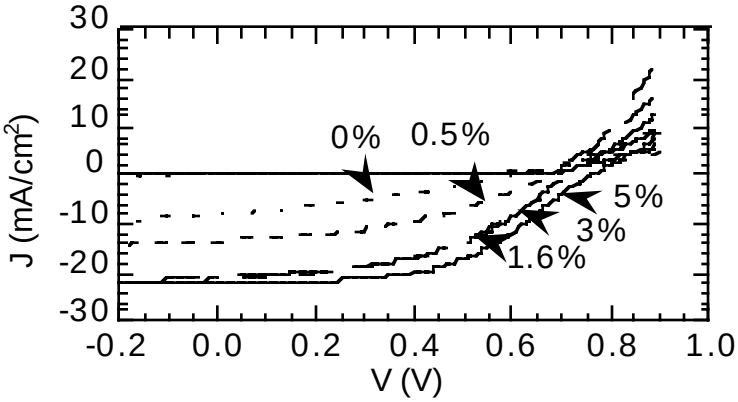

Figure 4-24. Dark and light J-V data for devices made from films heat treated for 30 min. at 400C in various HCl:Ar concentrations.

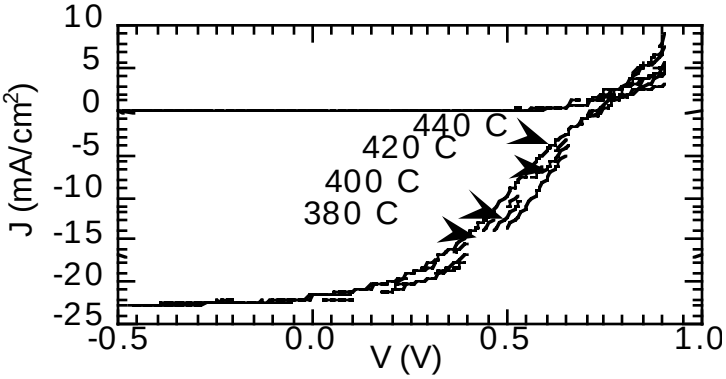

Figure 4-25 Dark and light J-V data for devices made from films heat treated for 30 min. in 5 % HCl at various temperatures.

4.4.6 Conclusions

Treatment of CdTe/CdS thin film structures in dilute mixtures of HCl vapor at 380˚C to 440˚C promotes similar microstructural changes in the structure to treatment with $CdCl_2$. While not yet optimized for high conversion efficiency, this shows promise as an alternative to treatments with $CdCl_2$. The structural properties are sensitive to both HCl concentration and treatment temperature. However, the device performance, particularly the short circuit current and fill factor, are highly

sensitive to HCl concentration but only slightly sensitive to treatment temperature. Achieving higher efficiency than demonstrated here will require exploration of a wider parameter space, including higher HCl concentration and multiple step treatments, such as HCl treatment followed by air treatment. Some of the difficulties associated with the use of hydrochloric acid as the vapor source and with using HCl:O_2 mixtures have been identified.

4.5 STRESS TESTING OF CdTe/CdS DEVICES

4.5.1 Introduction

The most delicate feature of the CdTe/CdS device is believed to be the low loss back contact. Low resistance contacting methods typically involve use of Te-rich interfaces or p-type semiconductors such as HgTe or ZnTe, or thin layers including small amounts of Cu [452-454]. Some devices subjected to stress testing or life testing display high series resistance and/or evidence of a reverse diode - both characteristics which could be attributed to the back contact. It has been reported [455] that reverse voltage bias at elevated temperature causes rapid degradation of device parameters and that this effect can be, at least, partially reversed by the application of a forward bias. Similar effects have been observed with devices produced in our lab. Analysis of the IEC light J-V curves indicated that there were at least two mechanisms responsible. Reversible effects included increases in series resistance and decreases in J_0 of the reverse diode upon application of reverse bias (with opposite changes upon forward bias); permanent effects included an additional increase in series resistance and a reduction in collected photocurrent [456, 457]. At this point it is not clear whether all CdTe devices display these effects or have the same sensitivity to these stresses.

4.5.2 Experimental Procedure

Devices evaluated in this study had the standard superstrate structure of glass/TCO/CdTe/CdS/contact. The sodalime glass/ SnO_2:F/CdS/CdTe supplied by Solar Cells Inc. was cut into 2.5 x 2.5 cm pieces from a 7200 cm^2 superstrate which had been coated and processed using SCI's normal procedures up to the point of completion of the post-deposition heat treatment [415]. The devices were completed using the "diffused Cu" back contact processing [446], sputter deposition of Mo contacts through a mask, mechanical scribing, application of a room temperature curing urethane insulator. Electrical contact was made using Ag epoxy (Acheson Electrodag MB80021) which was cured in Ar at 140 ˚C for ~10 minutes. In order to facilitate the subsequent depth profiling, in selected devices the Ag epoxy was applied only to the perimeter of the cell. Wire leads were soldered to the exposed SnO_2 pads using Indalloy solder #204. The leads were necessary to apply and maintain voltage bias on the devices during stressing and were used for making all J-V measurements.

Devices were not encapsulated, but all stressing was done inside a glove box with flowing N_2. Inside the glove box relative humidity was less than 2% at 50˚ C; oxygen content was not determined.

Prior to beginning the stress testing, devices have been screened to select those whose J-V data are analyzable. Devices exhibiting excessive series resistance (>10 Ω cm^2), shunting conductance (>1 mS/ cm^2), or hysteresis were rejected as were devices whose dark J-V characteristics could not be described with a simple diode (apparent diode quality factor ≤ 2.0). Minimum acceptable V_{OC} and FF were 0.75 V and 60%, respectively. A total of 16 devices meeting these criteria were selected for testing. The active area of these devices was estimated and set to 0.6 cm^2. Of these devices, four were stressed only with temperature (no electrical or light stress), two were stressed with temperature and electrical bias (-0.5 Volts and +5 mA/ cm^2) and the remaining 10 were

stressed with temperature, illumination (~70 mW/ cm^2) and electrical bias (see Table 4-11and Table 4-12).

Illumination was provided by tungsten filament spot lamps and was, therefore, quite "red" compared with the AM1.5 Global spectrum. The intensity was estimated from the short circuit current of the CdTe cells mounted in the stress test station.

Table 4-11 Electrical bias and temperature stress conditions for illuminated devices (~70 mW/ cm^2)

	82˚C	92˚C	112˚C
-0.5 V		√	
J_{SC}	√	√	√
R_L = 70 Ω	√		√
V_{OC}	√	√	√
+5 mA/ cm^2		√	

Table 4-12 Electrical bias and temperature stress conditions for devices stressed in dark

	72˚C	88˚C	104˚C
none	√	2	√
-0.5 V		√	
+5 mA/ cm^2		√	

J-V data were recorded at various intervals during the stress testing. In addition, devices were removed and room temperature J-V (at AM1.5 Global illumination and dark) and spectral response were also recorded prior to and at various times during stress testing . Total time under stress was 720 hrs.

4.5.3 Analysis

The most striking differences between the initial and final (720 hrs.) measurements occured in the J-V characteristics. These are examined in the context of a simple equivalent circuit containing a diode, a constant resistance (R_S) and a non-linear contact resistance (R_C).

$$V = \left(R_S + R_C\right)J + \left(\frac{AkT}{q}\right)Ln\left(\frac{J}{J_0}\right)$$

Equation 4-6

Hence the the effects of series resistance (R_S) and that of contact resistance (R_C) can be separated by examining the slope or derivative of the J-V characteristic.

$$\frac{dV}{dJ} = R_S + \left(\frac{AkT}{q}\right)\left(\frac{1}{J}\right) + \frac{d\left(R_C J\right)}{dV}$$

Equation 4-7

Equation 4-7 shows that contact resistance can be separated from simple series by examining a graph of dV/dJ vs. 1/J in forward bias or small 1/J (see Figure 4-27, Figure 4-29, Figure 4-31 and Figure 4-33).

4.5.4 Results

All of the devices held under stress conditions exhibited a reduction in V_{OC} and FF. These reductions could not be due to either shunting effects or a loss in light generated current.

4.5.4.1 Electrical Bias

There were major differences in the J-V characteristics of devices stressed with reverse bias (-0.5 V and J_{SC}) compared to those stressed at forward bias (+5mA/cm^2 and V_{OC}). Those held in reverse bias exhibited larger reductions in J_{SC}, V_{OC} and FF compared to those held in forward bias. Examination of the J-V curves (Figure 4-26 to Figure 4-29) help explain why. The increase in series resistance is larger for devices held at reverse bias. This can be seen in both the J-V and dV/dJ graphs and can account for at least some of the differences seen in V_{OC}, FF and J_{SC}.

In addition, there is another qualitative difference between devices stressed with forward or reverse bias; this is the appearance of a blocking contact resistance for devices held at forward bias. It can be seen most clearly in the dV/dJ graph of Figure 4-29. This is probably due to the development of a rectifying contact at the back of the CdTe.

4.5.4.2 Illumination

There were no obvious or consistent differences in the J-V characteristics of illuminated devices compared to those stressed in the dark.

4.5.4.3 Temperature

All of the changes noted previously were either accelerated or increased in magnitude when the temperature was increased (Figure 4-30 to Figure 4-33). This suggests that all of the mechanisms noted are thermally activated.

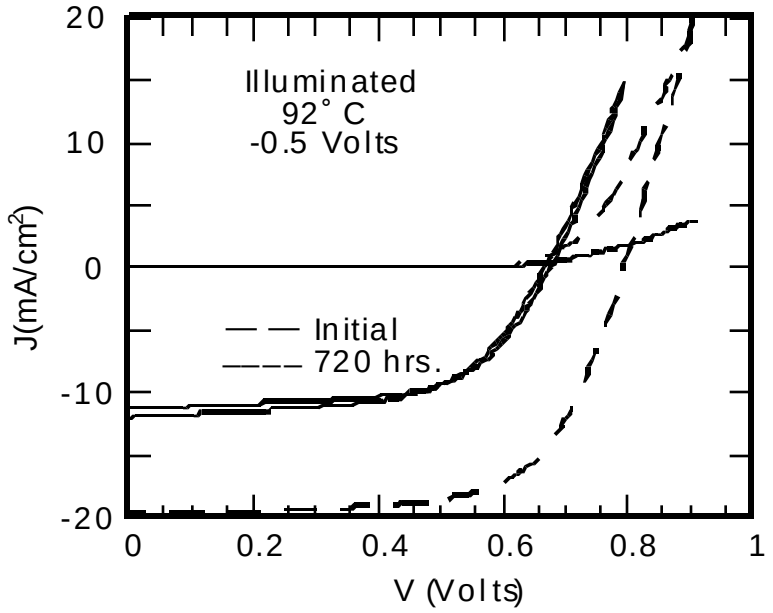

Figure 4-26 Light and Dark J-V characteristics before and after 720 hours stress at 92˚ C under illumination and -0.5V bias.

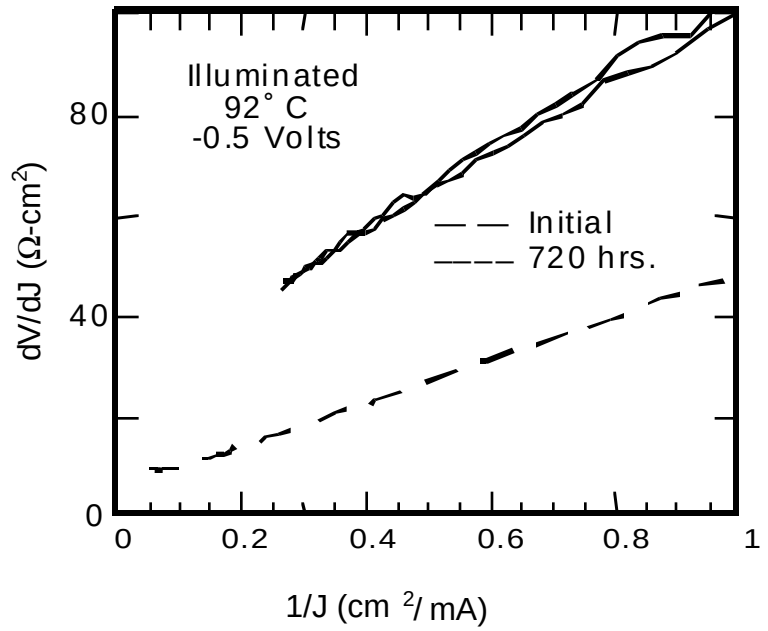

Figure 4-27 Dark dV/dJ vs. 1/J before and after 720 hours stress at 92˚ C under illumination and -0.5V bias.

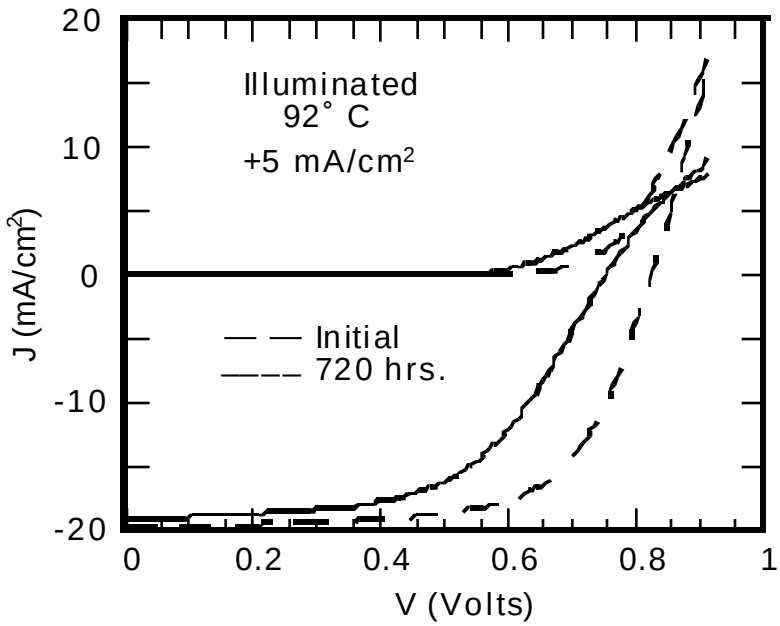

Figure 4-28 Light and Dark J-V characteristics before and after 720 hours stress at 92˚ C under illumination and +5mA/ cm^2 bias.

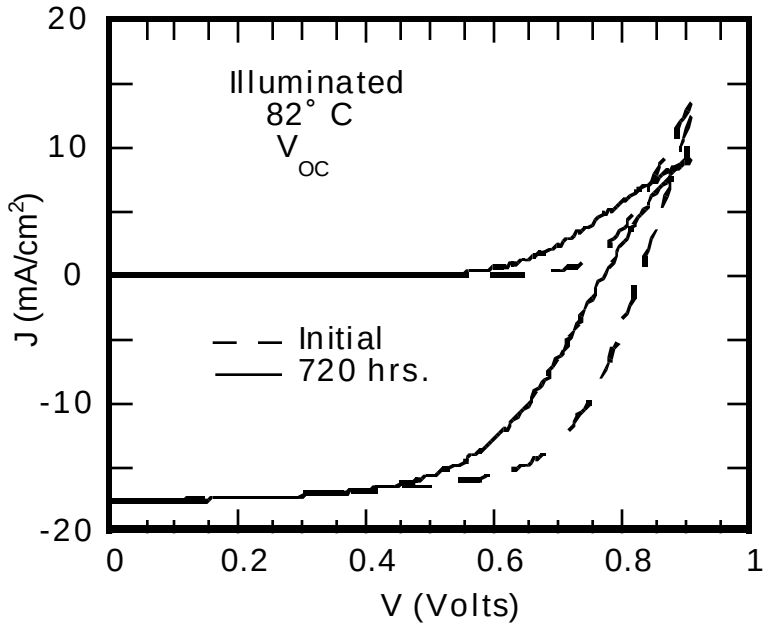

Figure 4-29 Dark dV/dJ vs. 1/J before and after 720 hours stress at 92˚ C under illumination and +5 mA/ cm^2 bias.

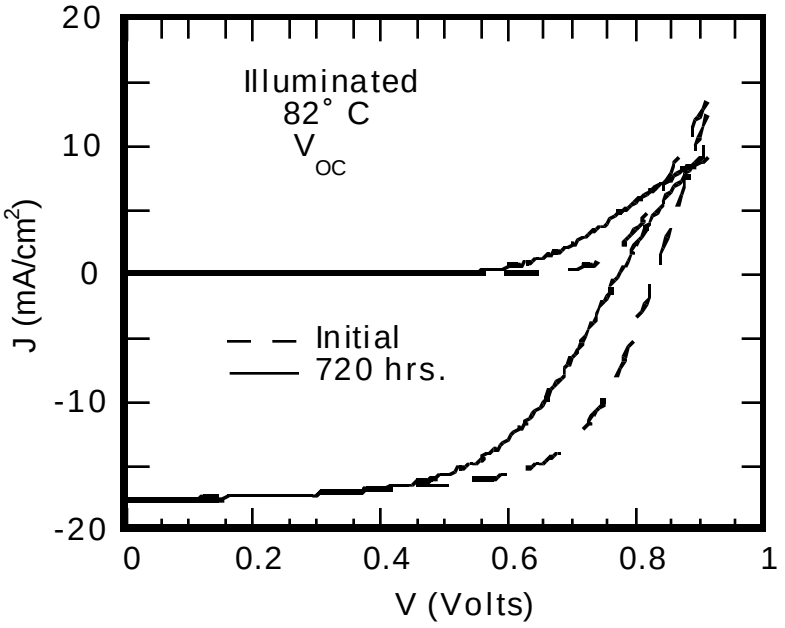

Figure 4-30 Light and Dark J-V characteristics before and after 720 hours stress at 82° C under illumination and held at V_{OC}.

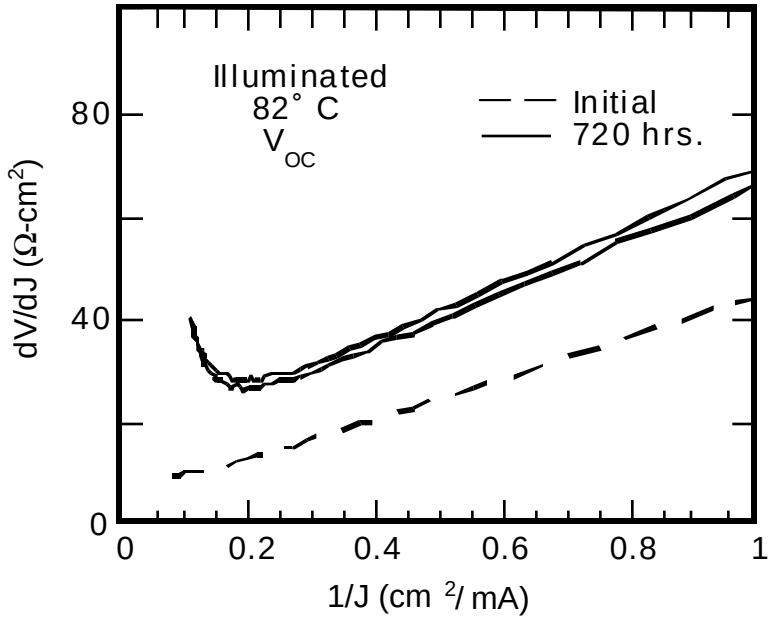

Figure 4-31 Dark dV/dJ vs. 1/J before and after 720 hours stress at 82° C under illumination and held at V_{OC}

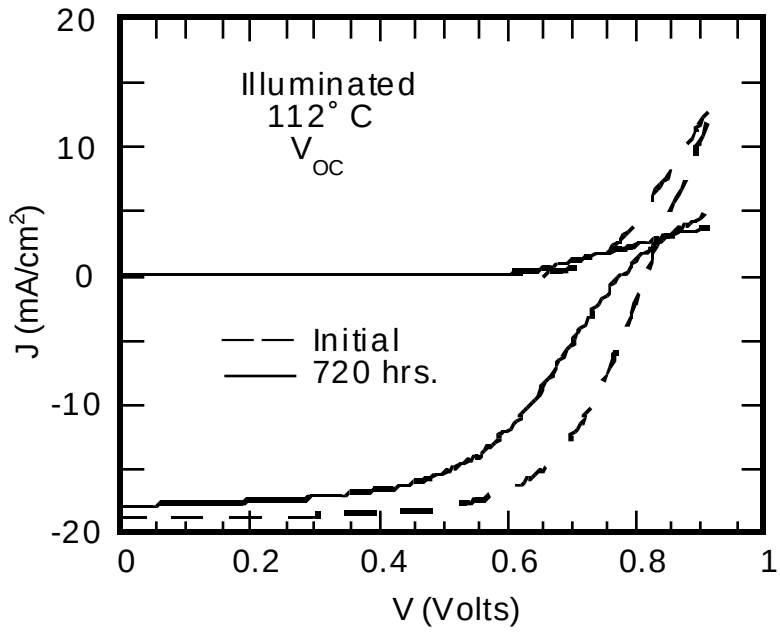

Figure 4-32 Light and Dark J-V characteristics before and after 720 hours stress at 112˚ C under illumination and held at V_{OC}

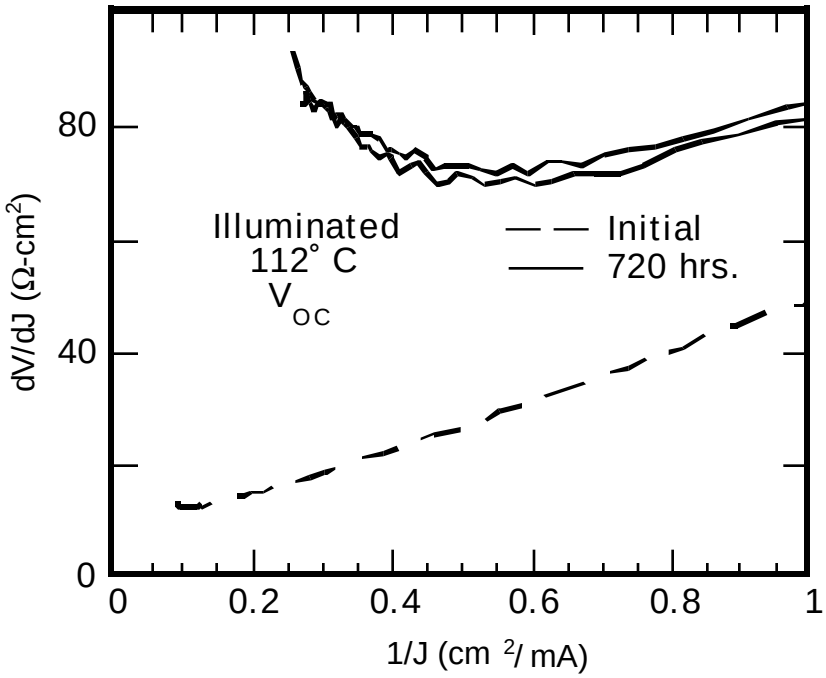

Figure 4-33 Dark dV/dJ vs. 1/J before and after 720 hours stress at 112˚ C under illumination and and held at V_{OC}.

4.5.5 Conclusions

In the specially prepared CdTe devices that have been subjected to stresses beyond normal operating conditions there appears to be changes that are associated with stress temperature and electrical bias. It is not clear whether there is a dependence on illumination level. One effect is promoted by reverse bias and affects primarily the bulk CdTe properties as indicated by the severity of the light-dark crossover of the J-V curves. Another effect is promoted by forward bias and results in the strengthening of a reverse diode. Finally there are changes in both the light generated current and J_0 whose magnitudes are also bias and light dependent. The data were recorded on a limited data set, 16 samples, and using a single method of device preparation. Additional experiments as well as other samples prepared by various groups are necessary to confirm or refute these results.

5. REFERENCES

5.1 SECTION 2 [$Cu(In,Ga)Se_2$]

201 R. W. Birkmire, J. E. Phillips, W. A. Buchanan, *et al*., Annual Subcontract Report, National Renewable Energy Laboratory, Golden, CO, (1996).

202 W. N. Shafarman, R. Klenk, and B. E. McCandless, J. Appl. Phys **79**, 7324 (1996).

203 W. N. Shafarman, R. Klenk, and B. E. McCandless, in *25th IEEE Photovoltaic Specialists Conference*, 1996), p. 763.

204 W. N. Shafarman, R. W. Birkmire, M. Marudachalam, *et al*., in *AIP Conference*, edited by C. E. Witt, M. Al-Jassim and J. M. Gee (AIP Press, Lakewood, CO, 1996), Vol. 394, p. 123-131.

205 M. Marudachalam, H. Hichri, R. W. Birkmire, *et al*., Appl. Phys. Lett. **67**, 3978-3980 (1995).

206 M. Marudachalam, H. Hichri, R. W. Birkmire, *et al*., in *25th IEEE Photovoltaic Specialists Conference*, 1996), p. 805.

207 W. N. Shafarman and J. E. Phillips, in *25th IEEE Photovoltaic Specialists Conference*, 1996), p. 917.

208 J. Hedstrom, H. Ohlsen, M. Bodegard, *et al*., in *23rd IEEE Photovoltaic Specialists Conference* (Institute of Electrical and Electronics Engineers, Louisville KY, 1993), p. 364.

209 J. R. Tuttle, M. A. Contreras, T. J. Gillespie, *et al*., Progress in Photovoltaics **3**, 235 (1995).

210 M. A. Contreras, J. Tuttle, A. Gabor, *et al*., in *24th IEEE Photovoltaic Spcialists Conference* (Institute of Electrical and Electronics Engineers, Waikoloa, HI, 1995), p. 68.

211 J. M. Stewart, W. S. Chen, W. E. Devaney, *et al*., in *7th Internatational Conference on Ternary and Multinary Compounds*, edited by S. K. Deb and A. Zunger (Materials Research Society, Pittsburgh, PA, 1987), p. 59.

212 K. Kushiya, Y. Ohtake, A. Yamada, *et al*., Jpn. J. Appl. Phys. **33**, 6599 (1994).

213 H. W. Schock, in *12th European Photovoltaic Solar Energy Conference* (H S Stephens & Assoc. UK, Amsterdam, The Netherlands, 1994), p. 944.

214 J. Kessler, S. Wiedeman, L. Russell, *et al*., in *25th IEEE Photovoltaic Specialists Conference*, 1996), p. 885.

215 J. Kessler, K. Velthaus, M. Ruckh, *et al*., in *6th Int. Photovoltaic Science and Engineering Conference* (Oxford and IBH, New Delhi, New Delhi, India, 1992), p. 1005.

216 W. E. Devaney, W. S. Chen, J. M. Stewart, *et al*., IEEE Trans. on Electron Devices **37**, 428 (1990).

217 B. Dimmler, H. Dittrich, R. Menner, *et al*., in *19th IUEEE Photovoltaic Specialists Conference* (IEEE, New York, New Orleans, LA, 1987), p. 1454.

218 B. Grzeta-Plenkovic, A. Popovic, B. Celustka, *et al*., J. Appl. Cryst. **13**, 311 (1980).

219 R. W. Birkmire, J. E. Phillips, W. A. Buchanan, *et al*., Annual Subcontract Report, National Renewable Energy Laboratory, Golden, CO, (1995).

220 D. Schmid, M. Ruckh, F. Grunwald, *et al*., J. Appl. Phys. **73**, 2902 (1993).

221 M. Roy, S. Damaskinos, and J. E. Phillips, in *20th IEEE Photovoltaic Specialists Conference* (IEEE, New York, Las Vegas, NV, 1988), p. 1618.

222 W. N. Shafarman and J. E. Phillips, in *22nd IEEE Photovoltaic Specialists Conference* (IEEE, New York, Las Vegas, NV, 1991), p. 934.

223 T. Walter, R. Menner, C. Koble, *et al*., in *12th European Photovoltaic Solar Energy Conference* (H. S. Stephens & Assoc., UK, Amsterdam, The Netherlands, 1994), p. 1755.

224 X. Liu and J. Sites, J. Appl. Phys. **74**, 1 (1993).

225 T. Negami, N. Kohara, M. Nishitani, *et al*., Appl. Phys. Lett. **67**, 825-827 (1995).

226 M. Eron and A. Rothwarf, Appl. Phys. Lett. **44**, 131 (1984).

227 M. Marudachalam, R. W. Birkmire, J. M. Schultz, *et al*., in *24th IEEE Photovoltaic Specialists Conference* (IEEE, Hawaii, Waikoloa, HI, 1994), p. 234.

228 S. Verma, T. W. F. Russell, and R. W. Birkmire, in *23rd IEEE Photovoltaic Specialists Conference* (IEEE, New York, Louisville, KY, 1993), p. 431.

229 R. Klenk and H. W. Schock, in *12th European Photovoltaic Solar Energy Conference* (H. S. Stephens & Assoc., UK, Amsterdam, The Nethelands, 1994), p. 1588.

230 T. Walter and H. W. Schock, Thin Solid Films **224**, 74 (1993).

231 R. J. Borg and G. J. Dienes, in *An Introduction to Solid State Diffusion* (Academic Press, Inc., 1988), p. 317-319.

232 W. Miller and L. C. Olsen, IEEE Trans. Elec. Dev. **ED-31**, 654 (1984).

233 W. N. Shafarman and J. E. Phillips, in *23rd IEEE Photovoltaic Specialists Conference*, 1993), p. 453.

234 F. Abou-Elfotouh, L. Kazmerski, T. Coutts, *et al*., J. Vac. Sci. Techn. **7**, 837 (1989).

235 J. Tuttle, J. Sites, A. Delahoy, *et al*., Progress in Photovoltaics **3**, 89 (1995).

236 Y. J. Lee and J. L. Gray, in *12th European Photovoltaic Solar Energy Conference* (H. S. Stephens & Assoc., UK, Amsterdam, The Netherlands, 1994), p. 1561.

237 H. Schade and Z. E. Smith, J. Appl. Phys. **59**, 1682 (1986).

238 M. Roy and J. E. Phillips, in *21st IEEE Photovoltaic Specialists Conference*, 1990), p. 743.

5.2 SECTION 3 [a-Si]

301 S. S. Hegedus, W. A. Buchanan, X. Liu, *et al*., in *25th IEEE Photovoltaic Specialists Conference* (IEEE, Washington, DC, 1996), Vol. 1, p. 1129.

302 S. S. Hegedus, W. A. Buchanan, E. Eser, *et al*., in *AIP Conference*, edited by C. E. Witt, M. Al-Jassim and J. M. Gee (AIP Press, Lakewood, CO, 1996), Vol. 394, p. 547-555.

303 S. S. Hegedus and X. Deng, in *25th IEEE Photovoltaic Specialists Conference* (IEEE, Washington, DC, 1996), Vol. 1, p. 1061.

304 R. W. Birkmire, J. E. Phillips, W. A. Buchanan, *et al*., Annual Subcontract Report, (National Renewable Energy Laboratory, Golden, CO, 1995).

305 R. W. Birkmire, J. E. Phillips, W. A. Buchanan, *et al*., Annual Subcontract Report, (National Renewable Energy Laboratory, Golden, CO, 1996).

306 S. S. Hegedus, H. Liang, and R. Gordon, in *AIP Conference*, edited by H. S. Ullal and C. E. Witt (AIP Press, Lakewood, CO, 1995), Vol. 353, p. 465.

307 M. Kubon, E. Boehmer, M. Gastel, *et al*., in *1st World Conference on Photovoltaic Energy Conversion*, 1994), p. 500.

308 R. R. Arya, R. S. Oswald, Y. M. Li, *et al*., in *1st World Conference on Photovoltaic Energy Conversion*, 1994), p. 394.

309 J. Hu and R. Gordon, Solar Cells **30**, 43 (1991).

310 H. Sakai, T. Yoshida, T. Hama, *et al*., Japan. J. Appl. Phys. **29**, 630 (1990).

311 J. Hu and R. Gordon, J. Electrochem. Soc. **139**, 2014 (1992).

312 M. Komakine, in *MRS Symposium*, 1990), Vol. 192, p. 69.

313 W. Luft, H. Branz, V. Dalal, *et al*., in *AIP Conference*, edited by H. S. Ullal and C. E. Witt (AIP Press, Lakewood, CO, 1995), Vol. 353, p. 81.

314 U. K Hoffman, , 1994).

315 A. Banerjee and S. Guha, in *Materials Research Society Symposium*, 1990), p. 57-62.

316 J. Morris, R. R. Arya, J. G. O'Dowd, *et al*., J. Appl. Phys. **67**, 1079-1087 (1990).

317 G. Tao, B. S. Girwar, G. E. N. Landweer, *et al*., in *Materials Research Society Symposium*, 1993), Vol. 297, p. 845-849.

318 E. Terzini, A. Rubino, R. DeRosa, *et al*., in *Materials Research Society Symposium*, 1995), Vol. 377, p. 681-686.

319 K. Hayashi, K. Masataka, A. Ishikawa, *et al*., in *IEEE First World Conference on Photovoltaic Energy Conversion* (IEEE, Waikoloa, HI, 1994), Vol. 1, p. 674.

320 M. Buchanan, J. B. Webb, and D. F. Williams, Appl. Phys. Lett. **37**, 213-215 (1980).

321 R. E. I. Schropp and A. Madan, J. Appl. Phys. **66**, 2027-2031 (1989).

322 W. Luft, H. M. Branz, V. L. Dalal, *et al*., in *AIP Conference* (AIP Press, 1994), p. 31-45.

323 M. Kubon, E. Boehmer, M. Gastel, *et al*., in *IEEE First World Conference on Photovoltaic Energy Conversion* (IEEE, Waikoloa, HI, 1994), p. 500.

324 J. Hu and R. Gordon, Solar Cells **30**, 437-450 (1991).

325 R. S. Sanchez and R. Williams, J. Appl. Phys. **54**, 2757-2760 (1983).

326 K. Itoh, H. Matsumoto, T. Kobata, *et al*., Appl. Phys. Lett. **51**, 1695 (1987).

327 B. Drevillon, S. Kumar, P. R. i. Cabarrocas, *et al*., Appl. Phys. Lett. **54**, 2088-2090 (1989).

328 F. Smole, M. Topic, and J. Furlan, in *IEEE First World Conference on Photovoltaic Energy Conversion* (IEEE, Waikoloa, HI, 1994), Vol. 1, p. 496.

329 H. Deckman, C. Wronski, H. Witzke, *et al*., Appl. Phys. Lett. **42**, 968 (1983).

330 G. Walker, R. Hollingsworth, and A. Madan, in *MRS Symposium*, 1987), Vol. 95, p. 527.

331 F. Leblanc, J. Perrin, and J. Schmitt, J. Appl. Phys. , 1074 (1994).

332 A. Banerjee and S. Guha, J. Appl. Phys. **69**, 1030 (1990).

333 A. Banarjee, K. Hoffman, X. Xu, *et al*., in *1st World Conference on Photovoltaic Energy Conversion* (IEEE, Waikoloa, HI, 1994), p. 539.

334 X. Deng, M. Izu, K. Narasimhan, *et al*., in *MRS Symposium*, 1994), Vol. 336.

335 R. E. I. Schropp, H. Meiling, W. G. J. H. M. v. Sark, *et al*., in *10th E.C. Photovoltaic Solar Energy Conference* (Kluwer Academic Publishers, Dordrecht, The Netherlands, Lisbon, Spain, 1991), p. 1087-1090.

336 H. Stiebig, A. Kreisel, K. Winz, *et al*., in *IEEE First World Conference on Photovoltaic Energy Conversion* (IEEE, Waikoloa, HI, 1994), Vol. 1, p. 603-606.

337 G. Tao, M. Zeman, and J. Metzalaar, in *First World Conference on Photovoltaic Energy Conversion* (IEEE, Waikoloa, HI, 1994), Vol. 1, p. 666-669.

338 V. Dalal, IEEE Trans. Electron Devices **ED-27**, 662 (1980).

339 S. Sze, *Physics of semiconductor devices* (John Wiley and Sons, New York, 1980).

340 M. Hack and M. Shur, J. Appl. Phys. **58**, 997 (1985).

341 H. Tasaki, W. Y. Kim, M. Hallerdt, *et al*., J. Appl. Phys. **63**, 550 (1988).

342 J. K. Arch, F. A. Rubinelli, J. Y. Hou, *et al*., J. Appl. Phys. **69**, 7057 (1991).

343 F. Smole and J. Furlan, J. Appl. Phys. **72**, 5964 (1992).

344 S. S. Hegedus and J. E. Phillips, in *First World Conference on Photovoltaic Solar Energy Conversion* (IEEE, Waikoloa, HI, 1994), Vol. 1, p. 654-657.

345 R. S. Crandall, J. Appl. Phys. **54**, 7176 (1983).

346 B. W. Faughnan and R. S. Crandall, Appl. Phys. Lett. **44**, 537 (1984).

347 R. R. Arya, A. Catalano, and R. S. Oswald, Appl. Phys. Lett. **49**, 1089 (1986).

348 R. S. Crandall and K. Sadlon, in *Materials Research Society Symposium*, 1989), Vol. 149, p. 423.

349 Y. Higaki, M. Aiga, S. Terazono, *et al*., Technical Digest of the International PVSEC **1**, 209 (1984).

350 K. Misiakos and F. A. Lindholm, J. Appl. Phys. **64**, 383 (1988).

351 R. Rocheleau, submitted to Progress in Photovoltaics (1997).

352 V. Chu, J. P. Conde, D. S. Shen, *et al*., Appl. Phys. Lett. **55**, 262 (1989).

353 R. Rocheleau, personal communication.

354 S. Wiedeman, J. Morris, and L. Yang, in *21st IEEE Photovoltaic Specialists Conference* (IEEE, Kissimmee, FL, 1990), Vol. 2, p. 1529.

355 H. Matsuura, A. Matsuda, H. Okushi, *et al*., J. Appl. Phys. **58**, 1578 (1985).

356 Y. Yamamoto, K. Nomoto, T. Okuno, *et al*., in *19th IEEE Photovoltaic Specialists Conference* (IEEE, New Orleans, LA, 1987), p. 901.

357 S. S. Hegedus, N. Salzman, and E. Fagen, J. Appl. Phys. **63**, 5126 (1988).

358 A. Mittiga, P. Fiorini, M. Falconieri, *et al*., J. Appl. Phys. **66**, 2667 (1989).

359 H. Sakai, T. Yoshida, S. Fujikake, *et al*., J. Appl. Phys. **67**, 3494 (1990).

360 J. R. Sites, H. Tavakolian, and R. A. Sasala, Solar Cells **29**, 39 (1990).

361 T. Glatfelter and J. Burdick, in *19th IEEE Photovoltaic Specialists Conference* (IEEE, New Orleans, LA, 1987), p. 1187.

362 C. R. Wronski and R. E. Daniel, Phys. Rev. **B-23**, 794 (1981).

363 M. Hack, S. Guha, and M. Shur, Phys. Rev. B **30**, 6991 (1984).

364 C.-D. Abel, H. R. Paes, and G. H. Bauer, in *10th European Conference of Photovoltaic Solar Energy Conversion*, Lisbon, Portugal, 1991), p. 161.

365 S. S. Hegedus and J. M. Cebulka, J. Appl. Phys. **67**, 3885 (1990).

366 L. Yang, A. Catalano, R. R. Arya, *et al*., Appl. Phys. Lett. **57**, 908 (1990).

367 E. Sauvain, J. Hubin, A. Shah, *et al*., Philosophical Magazine Letters **63**, 327 (1991).

368 I. Balberg, K. A. Epstein, and D. Ritter, Appl. Phys. Lett. **54**, 2461 (1989).

369 H. Pfleiderer, W. Kusian, E. Gunzel, *et al*., in *20th IEEE Photovoltaic Specialists Conference* (IEEE, Las Vegas, NV, 1988), p. 180.

370 J. Reichman, Appl. Phys. Lett. **38**, 251 (1981).

371 M. Stutzmann, W. Jackson, and C. C. Tsai, Phys. Rev. **B32**, 23 (1985).

372 D. Ritter, K. Weiser, and E. Zeldov, J. Appl. Phys. **62**, 4563 (1987).

373 E. Sauvain, P. Pipoz, A. Shah, *et al*., J Appl Phys **75**, 1722 (1994).

374 F. Wang and R. Schwarz, J. of Non-Crystalline Solids **198-200**, 423 (1996).

375 J. Yang, X. Xu, and S. Guha, in *1994 MRS Symposium*, 1994), Vol. 336, p. 687.

376 P. Chaudhuri, A. R. Middya, and S. Ray, in *6th International Conference on Photovoltaic Solar Energy Conversion*, 1992), p. 631.

377 J. Z. Liu, X. Li, P. R. i. Cabarrocas, *et al*., in *21st IEEE Photovoltaic Specialists Conference* (IEEE, Kissimmee, FL, 1990), p. 1606.

378 G. Conte, D. D. Sala, F. Galluzzi, *et al*., Semicond. Sci. Technol. **5**, 890 (1990).

379 G. H. Bauer, C. E. Nebel, and N.-D. Mohring, in *MRS Symposium*, 1988), Vol. 118, p. 679.

380 B. Faughnan, A. Moore, and R. Crandall, Appl. Phys. Lett. **44**, 613 (1984).

381 H. Okamoto, H. Kida, S. Nonomura, *et al*., J. Appl. Phys. **54**, 3236 (1983).

382 M. Isomura, T. Takahama, S. Tsuda, *et al*., Jpn. J. Appl. Phys. **32**, 1902 (1993).

383 R. Crandall and E. Schiff, in *AIP Conference*, edited by H. S. Ullal and C. E. Witt (AIP Press, Lakewood, CO, 1996), Vol. 353, p. 101.

384 Q. Wang, E. A. Schiff, and S. S. Hegedus, in *Materials Research Society Symposium*, 1994), Vol. 336, p. 365.

385 Q. Wang, R. Crandall, and E. Schiff, in *25th IEEE Photovoltaic Specialists Conference* (IEEE, Washington, DC, 1996), Vol. 1, p. 1113.

386 X. Xu, J. Yang, and S. Guha, in *23rd IEEE Photovoltaic Specialists Conference* (IEEE, Louisville, KY, 1993), Vol. 1, p. 971.

387 S. Guha, J. Yang, A. Banerjee, *et al*., in *AIP Conference*, edited by R. Noufi (AIP Press, Denver, CO, 1993), Vol. 306, p. 127.

388 R. Arya, *et al*., Final Report for Subcontract ZM-0-19003-1, (National Renewable Energy Laboratory, Golden, CO, 1994).

389 W. Luft, H. M. Branz, V. L. Dalal, *et al*., in *AIP Conference*, edited by R. Noufi and H. S. Ullal (AIP Press, Denver, CO, 1993), Vol. 306, p. 31.

390 J. Yang, X. Xu, A. Banerjee, *et al*., in *25th IEEE Photovoltaic Specialists Conference* (IEEE, Washington, DC, 1996), Vol. 1, p. 1041.

5.3 SECTION 4 [CdTe]

401 R. W. Birkmire, J. E. Phillips, W. A. Buchanan, *et al*., Annual Subcontract Report, (National Renewable Energy Laboratory, Golden, CO, 1996).

402 B. E. McCandless, H. Hichri, G. Hanket, *et al*., in *25th IEEE Photovoltaic Specialists Conference*, 1996), p. 781.

403 B. E. McCandless, R. W. Birkmire, D. G. Jensen, *et al*., in *14th NREL/SNL Photovoltaics Program Review* (AIP Press, Lakewood, CO, 1996), p. 647-654.

404 B. E. McCandless, L. V. Moulton, and R. W. Birkmire, Prog. Photovolt. Res. Appl. **5**, 249-260 (1997).

405 D. G. Jensen, B. E. McCandless, and R. W. Birkmire, in *MRS Meeting*, San Francisco, CA, 1996).

406 D. G. Jensen, B. E. McCandless, and R. W. Birkmire, in *25th IEEE Photovolaic Specialists Conference* (IEEE, Washington, DC, 1996), p. 773-776.

407 Y. Qu, P. V. Meyers, and B. E. McCandless, in *25th IEEE Photovoltaic Specialists Conference* (IEEE, Washgton, DC, 1996), Vol. 1, p. 1013-1016.

408 P. V. Meyers and J. E. Phillips, in *25th IEEE Photovoltaic Specialists Conference* (IEEE, Washington, DC, 1996), Vol. 1, p. 789-792.

409 B. E. McCandless and R. W. Birkmire, Solar Cells **31**, 527-535 (1991).

410 R. W. Birkmire, B. E. McCandless, and S. S. Hegedus, Int. J. Solar Energy **12**, 145-154 (1992).

411 J. Britt and C. Ferekides, Appl. Phys. Lett. **62**, 2851-2852 (1993).

412 J. Skarp, E. Anttila, A. Rautiainen, *et al*., Int. J. Solar Energy **12**, 137-142 (1992).

413 R. W. Birkmire, J. E. Phillips, W. A. Buchanan, *et al*., Annual Subcontract Report, (National Renewable Energy Laboratory, Golden, CO, 1994).

414 R. W. Birkmire, J. E. Phillips, W. A. Buchanan, *et al*., (National Renewable Energy Laboratory, Golden, CO, 1993).

415 T. X. Zhou, N. Reiter, R. C. Powell, *et al*., in *First World Conference on Photovolaic Energy Conversion* (IEEE, Waikoloa, HI, 1994), Vol. 1, p. 103-106.

416 R. W. Birkmire, H. Hichri, R. Klenk, *et al*., in *13th NREL Photovoltaics Program Review* (AIP Press, Lakewood, CO, 1995), p. 420-427.

417 B. E. McCandless and S. S. Hegedus, in *22nd IEEE Photovoltaic Specialists Conference* (IEEE, 1991), p. 967-972.

418 G. B. Harris, in *Phil. Mag.*, 1952), Vol. 43, p. 113.

419 H. P. Klug and L. E. Alexander, *X-Ray Diffraction Procedures* (John Wiley & Sons, New York, 1974).

420 B. E. McCandless, Y. Qu, and R. W. Birkmire, in *First World Conference on Photovoltaic Energy Conversion* (IEEE, 1994), Vol. 1, p. 107-110.

421 O. Knacke, O. Kubaschewski, and K. Hesselmann, (Springer-Verlag, Dusseldorf, 1991), p. 411.

422 I. Clemminck, M. Burgelman, M. Casteleyn, *et al*., in *22nd IEEE Photovoltaic Specialists Conference* (IEEE, Las Vegas, NV, 1991), p. 1114.

423 H. Matsumoto, A. Nakano, H. Uda, *et al*., Jpn. J. Appl. Phys. **21**, 800 (1982).

424 J. S. Lee, H. B. Kim, A. L. Fahrenbruch, *et al*., J. Electrochem. Soc. **134**, 1790 (1987).

425 J. S. Roh and H. B. Kim, J. Mat. Sci. **23**, 2267 (1988).

426 R. W. Birkmire, B. E. McCandless, and S. S. Hegedus, Int. J. Solar Energy **12**, 145 (1992).

427 S. A. Ringel, A. W. Smith, M. H. MacDougal, *et al*., J. Appl. Phys. **70**, 881 (1991).

428 S. K. Das and G. C. Morris, Solar Energy Materials and Solar Cells **28**, 305 (1993).

429 A. Nelson and S. Asher, (NREL.

430 B. E. McCandless and S. S. Hegedus, in *22nd EIII Photovoltaic Specialists Conference* (IEEE, Las Vegas, NV, 1991), p. 967-972.

431 R. W. Birkmire, S. S. Hegedus, B. E. McCandless, *et al*., in *AIP Conference*, edited by R. Noufi (AIP Press, Denver, CO, 1992), Vol. 268, p. 212-217.

432 S. H. Avner, *Introduction to Physical Metallurgy* (McGraw-Hill, New York, 1974).

433 M. M. Al-Jassim, F. S. Hasoon, K. M. Jones, *et al*., in *23rd IEEE Photovoltaic Specialists Conference* (IEEE, Louisville, KY, 1993), Vol. 1, p. 459.

434 W. A. Rachinger, Jour. Sci. Inst. **25**, 254 (1948).

435 C. Barrett and T. B. Massalski, *Structures of Metals* (Pergamon Press, London, 1980).

436 J. B. Nelson and D. P. Riley, Proc. Phys. Soc. **57**, 160 (1945).

437 A. Taylor and H. Sinclair, Proc. Phys. Soc. **57**, 126 (1945).

438 R. A. Young and D. B. Wiles, J. Appl. Cryst. **15**, 430-438 (1982).

439 K. Ohata, J. Saraie, and T. Tanaka, Jpn. J. Appl. Phys. **12**, 1641 (1973).

440 J. H. Brophy, R. M. Rose, and J. Wulff, *Thermodynamics of Structure* (Wiley and Sons, New York, 1966).

441 N. Nakayama, H. Matsomoto, A. Nakano, *et al*., Jpn. J. Appl. Phys. **19**, 703-712 (1980).

442 I. Clemminck, M. Burgelman, M. Casteleyn, *et al*., in *22nd IEEE Photovoltaic Specialists Conference* (IEEE, Las Vegas, NV, 1991), p. 114-119.

443 M. E. Ozsan, D. R. Johnson, D. W. Lane, *et al*., in *12th EC Photovoltaic Solar Energy Conversion Conference* (H. S. Stephens & Assoc., Bedford, UK, Amsterdam, The Netherlands, 1994), p. 1600-1603.

444 D. M. Oman, K. M. Dugan, J. L. Killian, *et al*., Appl. Phys. Lett. **67**, 1896-1899 (1995).

445 S. Nunoue, T. Hemmi, and E. Kato, J. Electrochem. Soc. **137**, 1248-1251 (1990).

446 B. E. McCandless, Y. Qu, and R. W. Birkmire, in *1st World Conf. on Photovoltaic Energy Conversion* (IEEE, Waikoloa, HI, 1994), Vol. 1, p. 107-110.

447 P. V. Meyers, C. H. Liu, and M. Doty, , US, 1989).

448 A. Compaan and A. Bhat, Int. J. Solar Energy **12**, 155-169 (1992).

449 F. Ullmann, *Ullmann's Encyclopedia of Industrial Chemistry* (VSJ Publishers, Deerfield Beach, FL, Weinheim, Fed. Rep. Germany, 1985).

450 (Wiley and Sons, New York, 1978), Vol. 12, p. 983-1011.

451 J. Saraie, H. Kato, N. Yamada, *et al*., Phys. Stat. Sol. **39**, 331-336 (1977).

452 A. F. Fahrenbruch, Solar Cells **21**, 399-412 (1987).

453 Y. S. Tyan, US patent (1980).

454 H. Uda, S. Ikegami, and H. Sonomura, Solar Energy Mater. **35**, 293-298 (1994).

455 T. X. Zhou, Final Technical Report, (National Renewable Energy Laboratory, Golden, CO, 1995).

456 A. Fahrenbruch and J. Sites, personal communications.

457 G. Stollwerk and J. R. Sites, in *13th European Photovoltaic Solar Energy Conference* (H. S. Stephens & Assoc., Bedford, UK, Nice, France, 1995).

6. ABSTRACT

This report describes results achieved during the a four year subcontract to develop and understand thin film solar cell technology related to $CuIn_{1-x}Ga_xSe_2$, a-Si and its alloys and CdTe. Accomplishments during this phase include:

- Fabrication of 15% efficient $CuIn_{1-x}Ga_xSe_2$ cells over a wide range of Ga compositions ($x \leq 0.5$).
- Fabrication of uniform single phase $Cu(Ga_xIn_{1-x})Se_2$ films and solar cells from the selenization of Cu-In-Ga precursors with the optical bandgap and device results expected for the precursor composition.
- Development of μc n-layers which have allowed fabrication of a-Si devices with efficiencies as high as 10%.
- Completion of the analysis and measurements that quantify the improvement in performance of a-Si solar cells due to optical enhancements from a wide range of TCO texture substrates and back reflectors.
- Development of uniform and reproducible vapor phase $CdCl_2$ treatments for CdTe/CdS films that have translated into greater consistency in device performance.
- Characterization of the CdTe-CdS alloy system at typical solar cell processing temperatures in order to elucidate the role of interdiffusion in CdTe/CdS-based solar cells.
- Development of a HCl vapor treatment of CdTe/CdS films that promote changes in the structure of the films similar to those treated with $CdCl_2$.

In addition to these in-house activities, IEC has maintained an active role in the collaboration with over ten different PV and thin film research and development organizations.